



This is a repository copy of *Climate-change versus landslide origin of fill terraces in a rapidly eroding bedrock landscape: San Gabriel River, California.*

White Rose Research Online URL for this paper:
<http://eprints.whiterose.ac.uk/108546/>

Version: Accepted Version

Article:

Scherler, D., Lamb, M. P., Rhodes, E. J. et al. (1 more author) (2016) Climate-change versus landslide origin of fill terraces in a rapidly eroding bedrock landscape: San Gabriel River, California. *Geological Society of America Bulletin* , 128 (7-8). pp. 1228-1248. ISSN 0016-7606

<https://doi.org/10.1130/B31356.1>

Reuse

Unless indicated otherwise, fulltext items are protected by copyright with all rights reserved. The copyright exception in section 29 of the Copyright, Designs and Patents Act 1988 allows the making of a single copy solely for the purpose of non-commercial research or private study within the limits of fair dealing. The publisher or other rights-holder may allow further reproduction and re-use of this version - refer to the White Rose Research Online record for this item. Where records identify the publisher as the copyright holder, users can verify any specific terms of use on the publisher's website.

Takedown

If you consider content in White Rose Research Online to be in breach of UK law, please notify us by emailing eprints@whiterose.ac.uk including the URL of the record and the reason for the withdrawal request.



eprints@whiterose.ac.uk
<https://eprints.whiterose.ac.uk/>

1 Climate-change versus landslide origin of fill terraces in a
2 rapidly eroding bedrock landscape: San Gabriel River, CA

3 Dirk Scherler^{1,2,3}, Michael P. Lamb¹, Edward J. Rhodes^{4,5}, and Jean-Philippe
4 Avouac¹

5 ¹Division of Geological and Planetary Sciences, California Institute of Technology, 1200
6 East California Boulevard, CA 91125, USA

7 ²GFZ German Research Centre for Geosciences, 14473 Potsdam, Germany

8 ³Freie Universität Berlin, Institute of Geological Sciences, Malteserstr. 74-100, 12249
9 Berlin, Germany

10 ⁴Department of Geography, University of Sheffield, Winter Street, Sheffield, S10 2TN, UK

11 ⁵Department of Earth, Planetary, and Space Sciences, University of California Los
12 Angeles, 595 Charles Young Drive East, Los Angeles, CA 90095, USA

13 Corresponding author: e-mail: scherler@gfz-potsdam.de; phone: +49 331 288-28646.

14 **ABSTRACT**

15 Fill terraces along rivers represent the legacy of aggradation periods that are most
16 commonly attributed to climate change. In the North Fork of the San Gabriel River, an
17 arid bedrock landscape in the San Gabriel Mountains, CA, a series of prominent fill
18 terraces were previously related to climate-change-induced pulses of hillslope sediment
19 supply that temporarily and repeatedly overwhelmed river transport capacity during the
20 Quaternary. Based on field observations, digital topographic analysis, and dating of
21 Quaternary deposits, we suggest instead that valley aggradation was spatially confined to
22 the North Fork San Gabriel Canyon and a consequence of the sudden supply of
23 unconsolidated material to upstream reaches by one of the largest known landslides in the
24 San Gabriel Mountains. New ¹⁰Be-derived surface exposure ages from the landslide
25 deposits, previously assumed to be early to middle Pleistocene in age, indicate at least

26 three Holocene events at ~8-9 ka, ~4-5 ka, and ~0.5-1 ka. The oldest and presumably
27 most extensive landslide predates the valley aggradation period, which is constrained by
28 existing ^{14}C ages and new luminescence ages to ~7-8 ka. The spatial distribution,
29 morphology, and sedimentology of the river terraces are consistent with deposition from
30 far-travelling debris flows that originated within and mined the landslide deposits. Valley
31 aggradation in the North Fork San Gabriel Canyon therefore resulted from locally
32 enhanced sediment supply that temporarily overwhelmed river transport capacity, but the
33 lack of similar deposits in other parts of the San Gabriel Mountains argues against a
34 regional climatic signal. Our study highlights the potential for valley aggradation by
35 debris flows in arid bedrock landscapes, provided sufficient supply of loose material,
36 downstream of landslides that occupy headwater areas.

37 **INTRODUCTION**

38 How landscapes respond to climate and other environmental changes is an
39 important issue in light of global climate change and anthropogenic changes in land use
40 (National Research Council, 2010). Most geomorphic research in this direction has so far
41 focused on soil-mantled landscapes and how changes in rainfall, vegetation cover, and
42 runoff lead to changes in sediment transport on hillslopes and by rivers (e.g., Knox, 1983;
43 Blum and Törnqvist, 2000). Far less inquiry has addressed how rapidly eroding, steep
44 bedrock landscapes respond to environmental changes (e.g., Riebe et al., 2001; DiBiase
45 and Lamb, 2013; Scherler et al., 2015). This is a shortcoming, because steep hillslopes
46 and higher mass fluxes have the potential for a greater and more rapid impact on
47 ecosystems and societies. The San Gabriel Mountains in Southern California, for
48 example, rate amongst the most rapidly uplifting mountains in the United States. Their
49 steep slopes and sensitivity to wildfires, flash floods, landslides, and debris flows account
50 for imminent hazards to nearby urban areas (e.g., Eaton, 1935; Lavé and Burbank, 2004;
51 Lamb et al., 2011; Kean et al., 2013). Assessing the potential risks that are associated
52 with climatic and other environmental changes requires understanding the controls on
53 sediment production and transport in these landscapes and how they change with time.

54 Because rates of sediment transport can be quite variable, observational records
55 are often too short to yield reliable trends. This is particularly true in semiarid to arid

56 environments, which are characterized by high rainfall, runoff, and discharge variability
57 (e.g., Molnar et al., 2006). In contrast, aggradational and degradational landforms provide
58 comparatively longer records of landscape change and usually integrate over short-term
59 variability. Amongst the most often used landforms for reconstructing landscape history
60 are river terraces, which are found all across the world. River terraces record the
61 geometry of previous valley floors that can be used to inform about sea level variations
62 (e.g., Merritts et al., 1994), or tectonic rates (e.g., Lavé and Avouac, 2001; Pazzaglia and
63 Brandon, 2001). Their formation is most often attributed to landscape-scale effects of
64 climate change (e.g., Leopold et al., 1964; Brakenridge, 1980; Knox, 1983; Weldon,
65 1986; Bull, 1991; Porter et al., 1992; Poisson and Avouac, 2004; Pazzaglia, 2013;
66 Scherler et al., 2015). However, other studies have shown that terraces can form even
67 during periods of steady downcutting, from intrinsic variations in river lateral migration
68 and meander cutoff (Davis, 1909; Merritts et al., 1994; Finnegan and Dietrich, 2011;
69 Limaye and Lamb, 2014; Limaye and Lamb, in review).

70 Traditionally, river terraces are sub-divided into strath and fill terraces. Whereas
71 strath terraces are cut into bedrock and typically capped with a thin veneer of sediment,
72 fill terraces represent remnants of valley fills that are often several tens to hundreds of
73 meters thick (e.g., Merritts et al., 1994; Pazzaglia, 2013). Most generally, valley fills form
74 when rivers switch from incision to aggradation. In uplifting landscapes that are far away
75 from sea-level changes, aggradation that is due to damming of a river by a landslide (e.g.,
76 Korup et al., 2006), or glacier (e.g., Montgomery et al., 2004; Scherler et al., 2014), can
77 usually be identified by a distinct spatial association of the fill and the dam. Valley fills
78 that are more regionally distributed are in most cases interpreted as resulting from fluvial
79 aggradation and incision in response to climate change (Bull, 1991).

80 Whether rivers incise, aggrade, or maintain a stable bed depends on the balance
81 between the river's transport capacity and the supply with sediments from hillslopes
82 (Lane, 1955; Bull, 1979; 1991). Temporal variations in transport capacity are mostly due
83 to changes in discharge and the slope of the bed, whereas both the amount and the caliber
84 of sediment that is supplied from hillslopes may vary. In static equilibrium, rivers neither
85 incise nor aggrade as their transport capacity is just in balance with the supply of
86 hillslope sediments. Any change of the system's variables may lead to departure from

87 equilibrium. For example, if discharge increases, everything else constant, the river
88 increases its transport capacity and incises. Incision should result in shallowing of the bed
89 gradient until the river reaches a new equilibrium. A decrease in discharge, or an increase
90 in the size or amount of sediment supply, on the other hand, would force a river to
91 aggrade and steepen its bed until shear stresses at the bed are high enough to transport all
92 of its material.

93 Based on detailed fieldwork and analytical tools available at that time, Bull (1991)
94 suggested that fill terraces in parts of the San Gabriel Mountains in Southern California
95 (Fig. 1) were formed by cycles of river aggradation and incision that occurred in response
96 to temporal variations in hillslope sediment supply and river transport capacity induced
97 by climatic changes. Moreover, Bull (1991) considered the San Gabriel Mountains as a
98 type locality for how an unglaciated, semiarid to subhumid mountain range has
99 responded to past climatic changes. Because the San Gabriel Mountains are mostly a
100 steep bedrock landscape (Lamb et al., 2011), rather than a soil mantled landscape, and
101 have slopes with angles greater than the angle of repose (DiBiase et al., 2012), they are
102 limited in their ability to have a much thicker soil mantle even under different Pleistocene
103 climatic conditions. Provided their apparent significance for understating how steep
104 bedrock landscapes respond to climate change, we have chosen the San Gabriel
105 Mountains for a detailed analysis with modern analytical tools and the aim to identify the
106 processes responsible for valley aggradation.

107 **STUDY AREA AND PREVIOUS WORK**

108 The San Gabriel Mountains constitute a transpressional basement block adjacent
109 to the Mojave segment of the San Andreas Fault (Fig. 1A) that comprises mostly
110 Precambrian igneous and metamorphic rocks as well as Mesozoic granites. It is bounded
111 in the south by the predominantly reverse-slip Sierra Madre-Cucamonga Fault Zone,
112 along which Holocene uplift rates of $\sim 0.5\text{--}0.9\text{ mm yr}^{-1}$ have been inferred, based on
113 offset landforms (Petersen and Wesnousky, 1994; Lindvall and Rubin, 2008). Uplift and
114 exhumation of the San Gabriel Mountains is thought to have initiated at ca. 12 Ma, and
115 accelerated at $\sim 5\text{--}7\text{ Ma}$ when the San Andreas Fault replaced the San Gabriel Fault as the
116 principal strike-slip fault in this region (Matti and Morton, 1993; Blythe et al., 2002).

117 Spatial differences in the onset and rate of uplift between different fault-bounded blocks
118 within the San Gabriel Mountains are thought to be responsible for a northwest-southeast
119 increase in landscape-scale relief that coincides with younger mineral cooling ages
120 (Blythe et al., 2000), higher ^{10}Be -derived erosion rates (DiBiase et al., 2010), as well as
121 enhanced fluvial erosion and more frequent landsliding (Lavé and Burbank, 2004).

122 The largest drainage in the San Gabriel Mountains is the San Gabriel River, with
123 an area of approximately 580 km^2 (Fig. 1A). Its East and West Fork follow the San
124 Gabriel Valley Fault for $>40\text{ km}$, whereas the North Fork of the San Gabriel River is
125 comparatively smaller (49 km^2). Along the lower $\sim 6\text{ km}$ of the North Fork San Gabriel
126 River, Bull (1991) identified four different flights of fill terraces, which he linked to a
127 regional terrace chronology with as many as nine different terrace levels, including sites
128 along the Lytle Creek in the northern San Gabriel Mountains, and the Arroyo Seco in the
129 western San Gabriel Mountains. The relative terrace chronology was substantiated by
130 three Holocene ^{14}C ages from the North Fork San Gabriel Canyon, and by correlation of
131 soil weathering stages (McFadden and Weldon, 1987) and acoustic wave speeds in
132 boulders (Crook, 1986) to dated terraces elsewhere in the western Transverse Ranges.
133 Based on this chronology, Bull (1991) interpreted the fill terraces in the North Fork San
134 Gabriel Canyon to represent four cycles of river aggradation and subsequent incision
135 (i.e., cut and fill cycles) that started at around 800, 120, 55, and 6 ka.

136 The North Fork San Gabriel Canyon stands out against the rest of the San Gabriel
137 Mountains with its abundance of fill terraces (Bull, 1991), at least in the lower part of the
138 catchment. The upper part of the catchment is dominated by two of the largest landslide
139 deposits in the San Gabriel Mountains, the Crystal Lake landslide ('CL' in Fig. 1B), and
140 the Alpine Canyon ('AC') landslide (Morton et al., 1989). Initial studies (Miller, 1926)
141 interpreted the Crystal Lake landslide as glacial deposits and thus evidence for
142 Pleistocene glaciation in the San Gabriel Mountains. This interpretation is probably
143 related to the fact that the landslide covers a considerable area in the uppermost reaches
144 of the North Fork San Gabriel Canyon. Subsequent studies however, suggest that the San
145 Gabriel Mountains have not been glaciated during recent glacial periods (Sharp et al.,
146 1959). Given an estimated minimum volume of $\sim 0.6\text{ km}^3$ (Morton et al., 1989), the
147 Crystal Lake landslide probably involved the collapse of a sizeable mountain flank. The

148 Alpine Canyon landslide is located downstream from the Crystal Lake landslide, and is
149 sourced by a small tributary east of the main stem. No dating of either landslide deposit
150 has been undertaken, but the most recent geological map of this area, assigns an early to
151 middle Pleistocene age to both landslide deposits (Morton and Miller, 2006).

152 Adjacent to the North Fork San Gabriel Canyon is the somewhat larger (73 km²)
153 Bear Creek Canyon, which otherwise has a very similar morphology (Fig. 1B). At similar
154 distance from the confluence with the West Fork, the Bear Creek lies approximately 500
155 m lower than the North Fork San Gabriel River. This circumstance is most likely the
156 result of the Crystal Lake landslide deposit (Fig. 1C). The outcropping rocks in both
157 catchments, the North Fork San Gabriel and the Bear Creek, generally comprise strongly
158 deformed basement rocks, including granitic and gneissic rocks, mylonites, cataclasites,
159 and abundant dikes (Morton and Miller, 2006). Due to their close proximity, and small
160 and similar size they experience similar climatic conditions and share a similar tectonic
161 and climatic history. If climate change caused fluvial aggradation in the North Fork San
162 Gabriel Canyon, it appears reasonable to expect similar geomorphic responses in the
163 adjacent Bear Creek Canyon. Throughout the remainder of the paper, we will thus
164 repeatedly compare the adjacent North Fork San Gabriel and the Bear Creek Canyons.

165 The restricted distribution of fill terraces in the San Gabriel Mountains is
166 surprising and atypical for climate change-related fill terraces, which typically are more
167 widely distributed (Knox, 1983). Furthermore, the spatial proximity of terraces and
168 landslides in the North Fork San Gabriel Canyon merits attention not previously granted.
169 Specifically, we ask the question whether this proximity is purely coincidental or related.
170 In the following, we will present field observations, analysis of high-resolution digital
171 topography, and cosmogenic exposure-age and luminescence dating that leads us to
172 consider an alternative mechanism for valley aggradation in the North Fork San Gabriel
173 Canyon and that holds implications for the response of bedrock landscapes to climate
174 change.

175 **DATA AND METHODS**

176 **Topographic analysis and field observations**

177 The spatial distribution of terraces and landslide deposits in the North Fork San
178 Gabriel and Bear Creek Canyons was documented by Bull (1991) and Morton and Miller
179 (2006). We complemented existing maps by our own field observations using a hand-
180 held GPS, topographic maps, and high-resolution aerial images. Because dense chaparral
181 restricts direct access to most of the landscape, we supplemented our fieldwork with
182 digital elevation model (DEM) analysis using MATLAB® and the TopoToolbox v2
183 (Schwanghart and Scherler, 2014). The 3-m resolution DEM is based on Interferometry
184 of Synthetic Aperture Radar (IfSAR) data, which was acquired during winter 2002/2003,
185 and is provided by the NOAA Coastal Services Center. Comparison with the 10-m
186 resolution National Elevation Dataset indicates that besides the influence of vegetation,
187 the IfSAR-derived DEM has higher errors in steep terrain (> 20 degrees).

188 Our digital mapping of terrace surfaces uses automatic identification of potential
189 terrace pixels in the DEM, based on surface gradient, curvature, and proximity to other
190 pixels of similar attributes. Subsequently we evaluated the results by comparison with
191 manually mapped terrace surfaces in the North Fork San Gabriel Canyon. It has been
192 pointed out that the spatial correlation of individual terraces can be misleading and
193 whenever possible should be substantiated with age dating (Merritts et al., 1994). In our
194 study area, however, distances between individual terraces are short (< 1 km) and along-
195 stream extents of some terraces large (> 200 m). This fact allows us to identify the
196 inclination of terraces surfaces and reconstruct valley bottoms along the stretch of the
197 studied valleys.

198 Although terrace surfaces ought to represent former valley floors, surface
199 processes modify their morphology after abandonment. In particular, dissection by
200 tributary rivers or colluvial deposition from adjacent hillslopes can modify terrace
201 surfaces and obscure the original valley floor gradient. We are aware that this
202 methodology therefore fails when it comes to heavily degraded terraces such as Bull's
203 (1991) T1 terrace. For comparing terrace surface gradients with the gradients of the
204 adjacent river channels, we projected each terrace pixel into a smooth flow path along the

205 valley and fitted a straight line to the distance-elevation pairs of all DEM pixels that
206 correspond to a given terrace surface. Although the smoothing of the flow path changed
207 its planview shape, we retained for each pixel on the flow path its distance along the river
208 from the unsmoothed flow path. This way, we avoid changes in the length of the flow
209 path (and thus gradient) through the smoothing procedure.

210 To estimate sediment caliber, we conducted grain-size counts within the present-
211 day river channel, on the flood plain, and along terrace outcrops, based on pace
212 measurements at equal steps of 1 m, without double counts, and recording the
213 intermediate axis of each grain. We acknowledge however that comparison of surface
214 measurements, where sorting of grain sizes can be expected (e.g., Parker and Klingeman,
215 1982), with those from outcrops is not straightforward. Our expectation is that grain size
216 counts from the modern channel may be biased by larger grains.

217 **Geochronological control**

218 **Post-IR IRSL dating**

219 To obtain age constraints on the aggradational episode in the North Fork San
220 Gabriel Canyon, we collected five samples for dating by single grain post-IR IRSL
221 (infrared-stimulated luminescence) of K-feldspar at two locations. Samples were
222 collected in steel tubes pushed horizontally into sandy units within vertical sediment
223 exposures. In-situ gamma spectrometer measurements were made at each sample
224 location, to determine the gamma dose rate contribution from the surrounding sediment.
225 Sediment beta dose rates were based on U, Th and K concentrations determined using
226 ICP- (Inductively Coupled Plasma) MS (Mass Spectrometry) and OES (Optical Emission
227 Spectrometry), corrected for grain size and water content attenuation. Cosmic dose rates
228 were estimated using present burial depths.

229 The luminescence dating approach adopted here is relatively new, and is
230 particularly suited for regions where quartz grains display low OSL sensitivity (Rhodes,
231 2015). A detailed description of the analytical procedures is provided in the
232 supplementary materials and in Rhodes (2015). The specific advantage of measuring
233 single grains is that sediments deposited rapidly, or close to their source, may contain
234 many grains that were exposed to insufficient daylight to fully reset their luminescence

235 signals. The use of single grains allowed us to isolate the grains with the minimum
236 equivalent dose (D_e) values by successively excluding grains with high D_e values until
237 the remaining population is consistent with an overdispersion value of $\leq 15\%$ (see
238 Rhodes, 2015, for details). The post-IR IRSL signal we used is less rapidly bleached by
239 sunlight than the quartz OSL signal (Rhodes, 2011), and our samples displayed many
240 grains that had very high dose values. These single grain post-IR IRSL age estimates are
241 based on results from a small proportion of grains with low dose estimates; the results of
242 many other grains with apparent old age estimates were rejected as representing grains
243 that were not exposed to light during, or immediately before, their transport and
244 deposition within the sampled sedimentary unit. In adopting this approach we follow
245 long-established luminescence dating procedures for the interpretation of single grain
246 results (Roberts et al., 1997). Where we observed no indications of post-depositional
247 sediment disturbance, we rigorously use the minimum dose values to estimate age. In our
248 presentation of the single grain results we only show grains with ages below 100 ka for
249 clarity, although grains with older, and often saturated ages were measured, too. A single,
250 very young grain that we interpret as introduced by bioturbation from a nearby burrow
251 we encountered during sampling, was excluded from age analysis for sample SG13-04.

252 **^{10}Be exposure dating**

253 We used in-situ produced ^{10}Be surface exposure dating of landslide boulders to
254 constrain the history of landslide occurrence in the North Fork San Gabriel Canyon. In
255 the field, we identified large (>3 m) and presumably stable boulders, i.e., wider than tall
256 and imbedded within the surrounding deposits, which showed no evidence of recent
257 spallation. We took our samples from the top surface of each boulder, and recorded their
258 average thickness and the orientation of the sampled surface, which are used for shielding
259 corrections. Separation and purification of Quartz grains, as well as chemical extraction
260 of Beryllium and isotopic measurements with an accelerator mass spectrometer was done
261 following standard procedures at the Purdue Rare Isotope Measurement Laboratory,
262 Purdue University. Table 3 lists the analytical sample results and the associated $1-\sigma$
263 uncertainties, based on the propagated uncertainties in the carrier concentration, two
264 process blanks ($^{10}\text{Be}/^9\text{Be}$ ratios of 5.5×10^{-15} and 3.8×10^{-15}), and the isotope

265 measurements. We calculated exposure ages from ^{10}Be concentrations using the
266 CRONUS-Earth online calculator v2.2 (Balco et al., 2008). The exposure ages we report
267 here, are based on the time-dependent version of the Lal (1991)/Stone (2000) production
268 rate scaling model ('Lm' in Balco et al., 2008). Topographic shielding was calculated
269 using the DEM and following Dunne et al. (1999). Shielding by snow or vegetation is
270 negligible in the San Gabriel Mountains and was not included. Frequent wild fires in the
271 San Gabriel Mountains could affect boulder surfaces by spallation, even if we don't see
272 any evidence for it today, which would bias exposure ages young. If significant, however,
273 spallation should lead to scatter in ages from different boulders obtained from the same
274 deposit, which as shown below is not the case for our study site.

275 **RESULTS**

276 **Morphology of the modern valley floor**

277 Compared to the Bear Creek Canyon and other rivers in the San Gabriel
278 Mountains, the modern valley floor in the North Fork San Gabriel Canyon is relatively
279 wide and covered with alluvium, suggesting that the valley still contains substantial
280 amounts of sediments that bury the bedrock river bed. In fact, the only notable bedrock
281 outcrop along the channel is at ~1 km distance from the confluence with the West Fork
282 San Gabriel River (Fig. 2). Here, the river has cut a ~17 m deep and ~60 m long bedrock
283 gorge into the eastern valley side, whereas 50 m farther west and at the same height as the
284 gorge, terrace deposits can be seen. It thus appears that during incision of the former
285 valley fill, the river did not reoccupy the same position within the valley but was trapped
286 in the newly formed epigenetic gorge (e.g., Ouimet et al., 2008). The gorge is the furthest
287 location upstream from the junction of the West Fork San Gabriel River that we observe
288 bedrock in the channel bed. This is in contrast to the Bear Creek Canyon, and most other
289 rivers in the San Gabriel Mountains, which are bedrock or have only a thin veneer (< 1
290 m) of alluvial cover (DiBiase, 2011).

291 With bankfull channel widths of 5-10 m, the active channel occupies only a small
292 portion of the surface of the modern valley floor, which is typically 100-200 m wide.
293 Even beyond the channel banks, the floodplain exhibits meter-scale relief, related to

294 gullies, boulder levees, and lobate boulder deposits (Fig. 3), which we infer to represent
295 mostly debris-flow deposits (cf., Whipple and Dunne, 1992).

296 **Longitudinal river profiles**

297 The longitudinal profile of a river has a characteristic shape that encodes
298 information about its evolution and along-stream changes in the forcing and boundary
299 conditions (Mackin, 1948; Hack, 1957). The downstream slope and upstream area of a
300 graded river typically obey power-law scaling (e.g., Flint, 1974) and under conditions of
301 topographic steady state, uniform lithology, climate, and rock uplift rates, the particular
302 scaling parameters are expected to be identical across a landscape (Wobus et al., 2006;
303 Kirby and Whipple, 2012). To analyze the scaling behavior of longitudinal river profiles
304 and to avoid issues with DEM-noise that may get exaggerated in slope data (e.g., Wobus
305 et al., 2006), we transformed the horizontal coordinate (distance) of channel elevation
306 data by upstream integration, and minimized the misfit between the resulting so-called χ -
307 plot and a straight line (Perron and Royden, 2012).

308 Analysis of the North Fork San Gabriel River and Bear Creek channels shows that
309 the degree to which the slope-area data obeys power-law scaling differs between the two
310 drainage networks (Fig. 4). In particular, the North Fork San Gabriel shows considerably
311 greater deviations of the individual profiles from a straight line than the Bear Creek.
312 Furthermore, the largest tributary of the North Fork San Gabriel River displays more
313 gentle slopes than the main stem river, resulting in lower elevations at similar distance
314 from their confluence. It should be noted however that this tributary (Bichota Canyon)
315 appears to follow a branch of the San Gabriel Valley Fault, which may partly explain the
316 unusual morphology. Quite different from this, the channel maintains a relatively
317 constant gradient across the epigenetic gorge and does not have a pronounced knickpoint
318 (Fig. 4), despite the strong lithological contrast between the bedrock and the valley fill,
319 and the abundance of waterfalls elsewhere in the San Gabriel Mountains (DiBiase et al.,
320 2014). Nevertheless, the peculiar profile of the North Fork San Gabriel River in its upper
321 reaches coincides with the extent of landslide deposits, suggesting that this part of the
322 drainage is not in topographic equilibrium. In contrast, the longitudinal profile of the
323 Bear Creek appears relatively graded for most of its length and the main stem and its

324 tributaries share rather similar channel steepness, although deviations from a graded
325 profile exist. These could be related to transient adjustments to changes in tectonic
326 forcing (e.g., DiBiase et al., 2014).

327 **Spatial distribution of terraces**

328 River terraces in the North Fork San Gabriel Canyon are exclusively found along
329 the lower 7 km of the valley and range in character and size from possible terrace
330 remnants a few meters wide and long, to well-developed flat terrace treads of up to
331 ~70,000 m² in area (Fig. 2). In the lower 4 km of the valley, we identified at least six
332 different terrace levels, with heights ranging between ~2-5 m and ~85 m above river level
333 (arl) (Fig. 5A). The most extensive level, at ~40 m arl, corresponds to Bull's (1991) T7
334 terrace. Lower terraces appear to be cut into the T7 valley fill. Higher terraces are less
335 frequent and more difficult to identify and to trace along the valley. At a distance of 4 to
336 5 km from the outlet, where the North Fork San Gabriel River turns northward, the T7
337 terrace surface decreases in elevation and eventually disappears farther upstream. The
338 highest upstream-located, well-developed terrace surface is at ~20 m above the river
339 bottom. Because of the similarity in extent, this terrace may represent the continuation of
340 T7, as already noted by Bull (1991), which would require a significant decrease in height
341 above the river. The T7 and younger terraces are clearly fill terraces, as shown at several
342 outcrops where the entire stratigraphy, from the modern valley floor to the top terrace
343 surface, is exposed. For the higher (older) terraces (T4 and T1 in Bull, 1991), this cannot
344 be ascertained due to the lack of exposure.

345 It is notable that the majority of terraces are located on the northwestern bank of
346 the North Fork San Gabriel River, and that they are most abundant between ~1 and 5 km
347 distance from the confluence with the West Fork of the San Gabriel River. This valley
348 reach coincides with a zone of subdued relief (Fig. 2) that traces the San Gabriel Valley
349 Fault Zone across the Bear Creek Canyon before branching off the main fault zone in a
350 northeastern direction to follow a fault branch along the North Fork San Gabriel and
351 Bichota Canyons (Jennings and Bryant, 2010). Surprisingly, however, we found no
352 terraces in Bichota Canyon.

353 River terraces are also abundant in the Bear Creek Canyon and predominantly
354 found in the lower ~8-9 km of the valley (Fig. 2). In contrast to the North Fork San
355 Gabriel Canyon, all terraces that we observed in Bear Creek Canyon were strath terraces,
356 with fluvial gravels of a few meters thickness, at most, resting on top of bedrock. Unlike
357 terraces in the North Fork San Gabriel, terraces in the Bear Creek Canyon have similar
358 heights and define at least two pronounced terrace levels at ~35 m and ~77 m ahl (Fig.
359 5B). The higher level is more abundant in the upper reaches of the Bear Creek Canyon
360 and in many places the terrace surfaces can be seen to transition into gentle-sloping
361 colluvial hillslopes (Fig. 2). Other terrace levels are less well expressed or
362 indistinguishable from the two more pronounced levels.

363 River terraces also exist along the West Fork San Gabriel River but their
364 distribution is more restricted (Fig. 2). Since its construction in 1939, the San Gabriel
365 Dam, which is located ~3.5 km downstream from the confluence of the East and West
366 Fork of the San Gabriel River, has forced the river to aggrade its bed, as far as 3 km
367 upstream from the confluence. Beyond this distance the only terraces we observed are
368 strath terraces of relatively small extent (~50 m x 50 m). We extrapolated the two most
369 pronounced terrace surfaces in the Bear Creek and North Fork San Gabriel Canyons into
370 the West Fork, to examine whether they line up with other distinct terrace levels (Fig.
371 5C), although we acknowledge that correlating terraces across watersheds by elevation
372 can be problematic. The lower terrace level in the Bear Creek Canyon (~35 m ahl) is very
373 close ($\Delta z < 5$ m) to two terrace levels in the West Fork. For the upper terrace level (~70
374 m ahl), the exact position of the confluence with the West Fork is not well constrained,
375 but it appears poorly aligned with higher terrace levels in the West Fork Canyon. The two
376 most pronounced terrace levels in the North Fork San Gabriel Canyon align only partly
377 with corresponding terrace levels in the West Fork. Whereas the T5 terrace level in the
378 North Fork San Gabriel Canyon might be related to the upper terrace level in the Bear
379 Creek Canyon, the widely distributed T7 terrace level appears to be distinctly different
380 from any terrace surfaces in the Bear Creek Canyon.

381 **Terrace versus river gradients**

382 Present-day river gradients in the North Fork San Gabriel cluster around 0.05 and
383 0.08, corresponding to reaches below and above the junction with Bichota Canyon,
384 respectively (Fig. 6). Terrace surface gradients along the channel axis direction occupy a
385 wider range of values, ~0-0.1, and are on average slightly less steep than the active
386 channel. River gradients in Bear Creek Canyon are typically lower, between 0.03 and
387 0.06, although upstream parts of the river steepen to 0.1. Terrace gradients in Bear Creek
388 occupy a similar range as those in the North Fork San Gabriel, but appear on average
389 somewhat gentler than the corresponding river gradients. In both canyons, the shallowest
390 gradients are typically associated with terrace surfaces whose true dip is highly oblique to
391 the valley axis, and which have a rather small downstream elongation, that is, their
392 across-valley extent is large relative to their down-valley extent. These attributes indicate
393 that the measured surface gradients are associated with relatively higher uncertainties.

394 **Valley fill reconstruction**

395 Based on the spatial distribution of T7 terrace surfaces in the North Fork San
396 Gabriel Canyon, we estimated the elevation of the corresponding former valley fill
397 surface (Fig. 5A). After projecting terrace pixels into the flow path, we sought a visual fit
398 of all T7 terraces with piecewise splines. The along-valley distance of each terrace pixel
399 was obtained by creating a 1-km wide swath that follows the valley using functions from
400 the TopoToolbox v2 (Schwanghart and Scherler, 2014). The resulting one-dimensional
401 valley fill surface was extended laterally by assuming across-valley constant heights,
402 again using the 1-km wide swath. Finally, each pixel was assigned the maximum value of
403 the valley fill surface and the modern topography (cf., Scherler et al., 2015). Subtracting
404 the present-day topography from the valley-fill surface yields an estimated volume of
405 ~0.034 km³ of material that has been eroded since abandonment of the T7 surface (Fig.
406 7A). We also estimated the bedrock elevation beneath the valley fill, by projecting the
407 adjacent hillslopes at an angle of 35° into the subsurface. This hillslope angle is
408 representative for bedrock hillslopes in the North Fork San Gabriel and Bear Creek
409 Canyons (Fig. 2; DiBiase et al., 2010). Although this approach is rather crude and misses
410 details of the true bedrock surface, it allows us to obtain a rough estimate of the volume

411 of material that is still stored in the valley. By subtracting the estimated bedrock elevation
412 from the reconstructed T7 surface, we estimate the total volume of the valley fill to be of
413 the order $\sim 0.1 \text{ km}^3$ (Fig. 7B). The estimated depth to bedrock increases with upstream
414 distance from the outlet of the North Fork San Gabriel and reaches its maximum depth of
415 $>100 \text{ m}$ below the present-day valley bottom near the junction with the Bichota Canyon.
416 Farther upstream, valley narrowing results in a decrease of the estimated depth to bedrock
417 to $<50 \text{ m}$, followed by another increase towards the transition from the terraces to the
418 landslide deposits.

419 **Terrace stratigraphy**

420 At small spatial scales (cm), the sediments exposed at terraces outcrops do not
421 show any stratification (Fig. 3e,f). At larger spatial scales, coarse-grained poorly sorted
422 lenses of subrounded to subangular boulders and cobbles that are roughly $\sim 0.5\text{-}2 \text{ m}$ thick
423 and 20 m wide are vertically separated by $\sim 2 \text{ m}$ from finer-grained matrix supported
424 deposits (Fig. 8b). The transition between the coarse-grained lenses and the fine-grained
425 deposits is gradual and not well defined. These assemblages look similar to the levee-
426 snout topography on the modern flood plain. At two locations along the North Fork San
427 Gabriel River we measured the dip of the coarse-grained lenses from outcrops that
428 parallel the valley trend using a laser range finder (Fig. 2). Near the upstream end of the
429 terraces at 6.3 km distance from the outlet, these lenses dip at $0.11\text{-}0.12$ ($n=2$), which is
430 slightly steeper than the gradient of the river (~ 0.1) and of the terrace surface (~ 0.07). At
431 a distance of 4.7 km from the outlet, the lenses dip at $\sim 0.05\text{-}0.06$ ($n=3$), which in this case
432 is less than the gradient of the river (~ 0.08) and of the terrace surface (~ 0.08).

433 Fluvial response to climate change is expected to produce grain size variations
434 (Armitage et al., 2011). The grain size of the sediment within the terraces however, is not
435 markedly different from that of sediment in the modern channel and on the flood plain, or
436 from sediment on the flood plain of the Bear Creek (Fig. 9). Median grain sizes (D_{50}) of
437 the terrace deposits range between 22 and 60 mm in diameter. Although our grain-size
438 measurements from the active channel and flood plain of the modern valley floor indicate
439 on average coarser grains compared to the terraces, this difference may simply be due to
440 the effect of sorting, in which both debris-flow deposits and river beds tend to have

441 coarser grains near their tops (e.g., Parker and Klingeman, 1982; Takahashi, 2014).
442 Significant variability in grain sizes was also observed by DiBiase and Whipple (2011) in
443 a study covering the entire San Gabriel Mountains, where median grain sizes (D_{50}),
444 ranged between ~22 and 180 mm. From Fig. 8b it is clear that significant grain-size
445 variations exist within individual terrace deposits; a fact that is also reflected in the
446 different grain size distributions that we and Bull (1991) obtained from the same T3
447 deposit (Fig. 9). Finally, it is notable that we observed by far the largest grain sizes in our
448 survey of the active channel immediately downstream of the landslide deposits. Bull
449 (1991) reported similar values from an active channel ('SC'), but the location was not
450 documented.

451 **Post-IR IRSL depositional ages**

452 The three available ^{14}C ages that were obtained by Bull (1991) stem from a 40 m
453 high and ~150 m wide terrace outcrop at Tecolote Flat (Fig. 2). This is a key locality
454 where the hypothesis of multiple cut-and-fill events can be tested, because the outcrop
455 exposes gravels that are associated to the T7 terrace, and according to Bull (1991)
456 presumably also older (T3) deposits that were buried by the T7 gravels and are now re-
457 exposed. Due to the poor sorting of the sediments, we found it difficult to pin down the
458 contact between these units at the outcrop, whereas at greater distance differences in
459 grain size and color are apparent (Bull, 1991) (see Figure S1 in the supplementary
460 material). In the lower-left part of Fig. 8B, the dashed line follows a ledge in the modern
461 face of the cliff that is decorated with vegetation (cf., Figure S1), and raises the
462 impression that the T3 deposit is actually adjoining the T7 deposit laterally and therefore
463 younger.

464 To shed light on stratigraphic order of these deposits, we collected three IRSL
465 samples at Tecolote Flat. The first two (SG13-01 and -02) stem from the apparent T3
466 deposit, close to the base of the terrace (Fig. 8B), and are vertically separated by only ~1
467 m. With depositional ages of 7.4 ± 0.8 ka (SG13-01) and 7.5 ± 0.7 ka (SG13-02; Fig. 10),
468 both samples yielded ages that are statistically indistinguishable from Bull's (1991) ^{14}C
469 ages of 7.3 ± 0.1 ka and 7.6 ± 0.2 ka that stem from the T7 deposit to the left of the T3
470 deposit. Our third sample (SG13-03) was collected from the T7 deposit at a

471 stratigraphically higher, hence younger position, compared to the Bull's (1991) ^{14}C
472 samples and is located to the right of the T3 deposit. This sample displays very poor
473 bleaching, with only a single result representing a well-separated minimum age peak at
474 5.6 ± 1.3 ka (SG13-03; Fig. 10). This single result is from 116 grains that provided finite
475 age results of 400 measured in total for this sample. Note that given the significant $1-\sigma$
476 uncertainty, this sample may be consistent in depositional age with the two lower samples
477 from this exposure, or may have been deposited somewhat later. Because the population
478 of old grains is very similar to the samples SG13-01 and -02, we think that this sample is
479 just very poorly bleached, due to insufficient exposure to sunlight. Therefore, our new
480 IRSL ages agree with the available ^{14}C ages by Bull, and do not support an old (T3)
481 valley fill covered by the T7 terrace. An alternative explanation is that the T3 deposit
482 truly adjoins the T7 deposit laterally but has been eroded in its central part exposing T7
483 material that we dated. However, this scenario appears unlikely as coarse-grained layers
484 can be traced continuously across the face of the presumable T3 deposit. More samples
485 and observations are needed to unravel the stratigraphic context of these units.

486 The other two samples were taken from a terrace outcrop near the uppermost limit
487 of the fill terraces, close to the first occurrence of landslide deposits (Fig. 2). These
488 samples yielded again very few grains that we considered potentially bleached. The most
489 likely age of SG13-04 is 8.2 ± 1.0 ka and based on only 4 grains. We discarded one grain
490 that gave an even younger age of $\sim 2 \pm 1$ ka, which we think might be related to a bird
491 burrow that we encountered at the sampling site. The stratigraphically higher, hence
492 younger sample SG13-05 gave an age of 7.0 ± 1.7 ka, based on only 2 grains. Again, the
493 population of old grains in these two samples is very similar to that of the other samples,
494 which we interpret to be the result of incomplete bleaching.

495 **Landslide deposits**

496 **Crystal Lake landslide**

497 Based on their morphology and distribution, we distinguished at least three
498 different landslide deposits in the upper North Fork San Gabriel Canyon (Fig. 11). The
499 most extensive deposit belongs to the Crystal Lake (CL) landslide and covers an area of
500 ~ 7 km², situated between ~ 1000 and ~ 2000 m elevation. Approximately half of the area

501 lies at an elevation above 1600 m and constitutes a broad, pan-shaped alluvial surface,
502 which is surrounded by bedrock hillslopes that transition into scree slopes, debris flow
503 channels, and debris fans. Several smaller intermittent creeks occupy this surface and
504 leave it in its southeastern corner, where they merge to form the Soldier Creek. Large
505 parts of this upper level appear to constitute reworked landslide deposits and active
506 fluvial and debris flow depositional areas, which prevented us from collecting any
507 samples there. Crystal Lake itself is confined to a small topographic depression in the
508 southwestern corner of the upper level, adjacent to steep bedrock hillslopes in the west
509 and an elongated, north-to-south trending topographic ridge in the east. This so-called
510 Sunset Ridge can be traced for >3 km as a distinct morphological feature that is
511 associated with large and angular, gneissic-granitic boulders on its surface. Although no
512 clear detachment scars can be seen in the field, the Sunset Ridge, and the morphology of
513 the surrounding hillslopes suggests that the source areas of the Crystal Lake landslide
514 were located to the north and east of this upper level (Morton et al., 1989). Below the
515 upper low-relief area is another, less extensive one, which is located at elevations of
516 around 1400 m. These two levels are separated by a topographic step, which features a
517 ~500 m wide slump along its steepest part. West of the lower level, additional gentle-
518 sloping surfaces are located ~150-200 m higher, but farther to the south they join into the
519 same level. Below ~1350 m, the Crystal Lake landslide deposit is exposed on steep
520 hillslopes and confined on either side by the Coldbrook and Soldier Creeks, which
521 actively incise headwards, thereby creating pronounced erosional escarpments.

522 We collected 7 samples from boulders that we associate to the Crystal Lake
523 landslide for surface-exposure dating with ^{10}Be . Three of the samples (DS103, DS106,
524 and DS406) stem from boulders situated on the upper level, but at opposing sides of the
525 valley. All three samples yield ages that overlap within uncertainties (Fig. 11, Table 3),
526 with an average age of $\sim 3.9 \pm 0.2$ ka. Three more samples (DS203, DS404-405) that we
527 collected from boulders on the lower low-relief area yielded similar ages, with an average
528 age of $\sim 4.4 \pm 0.25$ ka. The slightly older age is due to sample DS203 that gave an age of
529 $\sim 5.0 \pm 0.5$ ka, which may be due to inheritance as an adjacent boulder yielded an age of
530 4.0 ± 0.4 ka (DS405). Our last sample (DS206) from the Crystal Lake landslide stems
531 from the gentle-sloping area that is located west of and ~150 m above the lower three

532 samples. This boulder has an exposure age of $\sim 33 \pm 3$ ka. As this is our only sample from
533 the Crystal Lake landslide with an age markedly older than mid-Holocene, it is difficult
534 to provide a concluding explanation. Because the boulder rests on relatively low sloping
535 terrain that is at a markedly higher elevation than the areas farther to the east, it may be
536 that these surfaces represent remnants of an older deposit.

537 **Alpine Canyon landslide**

538 The Coldbrook and Soldier Creeks join at the toe of the Crystal Lake landslide
539 and flow for another ~ 500 m across a gentle-sloping alluvial reach before they dissect the
540 lower part of the Alpine Canyon landslide. The Alpine Canyon landslide covers an area
541 of ~ 1.3 km², between ~ 900 and ~ 1800 m elevation, and is steeper and narrower than the
542 Crystal Lake landslide. The canyon's drainage originates at ~ 2300 m near the highest
543 point of the catchment, and is first manifested as a debris flow channel with a slope of
544 ~ 0.62 that has been carved ~ 50 m into the bedrock (Fig. 12). Near ~ 1700 m the channel
545 encounters the landslide deposit, marked by a pronounced topographic step (Fig. 12B).
546 Between an elevation of ~ 1500 and 1300 m, the channel has a slope of ~ 0.23 and is
547 paralleled by an approximately 2 km long topographic ridge that straddles the
548 southeastern valley side. This ridge is quite similar to the Sunset Ridge at the Crystal
549 Lake landslide, although it is less vegetated and bounded by a steep slope at the valley
550 side. The area between the ridge and the hillside occupies a sub-horizontal, hummocky
551 surface that is mantled by coarse and angular boulders (Fig. 13B). This boulder field
552 extends for more than 1 km, parallel to the canyon, and terminates at an east-west striking
553 interfluvial, suggesting that landslide material overtopped to the south. Along the lower 3
554 km, the Alpine Canyon landslide has an average surface gradient of approximately 0.13
555 and develops a slightly convex surface that has been dissected by the intermittent Alpine
556 Canyon Creek. Between the transverse profiles 'e' and 'f' in Fig. 12, the so-called
557 Clouburst Canyon is cut by approximately 35 m into the landslide surface (Fig. 14) and
558 bounded by hillslopes with slope angles of 40° and more.

559 We collected five samples from boulders that we associate to the Alpine Canyon
560 landslide. Three of the samples (DS502-504) stem from the boulder field in the
561 southeastern corner of the landslide, at an elevation of ~ 1250 m (Fig. 13B). The three

562 ages overlap within uncertainties and yield an average age of 0.7 ± 0.2 ka. The other two
563 samples (DS402-403) stem from boulders from the surface of the main landslide deposit
564 near Clouburst Canyon and have similar ages of $\sim 0.9\pm 0.1$ ka. For a maximum landslide
565 age of $\sim 1,000$ years, the 35 m of incision at Clouburst Canyon yields a time-averaged
566 incision rate of 35 mm yr^{-1} .

567 The lowermost landslide deposit is found near the toe of the Alpine Canyon
568 landslide, which led Morton et al. (1989) to suggest that it is part of the same landslide.
569 However, the deposit, which has an area of $\sim 0.4 \text{ km}^2$ and an average elevation of ~ 950 m,
570 is ~ 50 m higher than the adjacent surface of the Alpine Canyon landslide, precluding a
571 common origin. Similar to the terminal part of the Alpine Canyon landslide, the river-
572 facing slope forms a steep ($>30^\circ$) erosional escarpment and a gentle-sloping surface that
573 dips away from the river towards the western hillslopes, somewhat resembling the
574 morphology of a large levee. Much of the northern half of this deposit has undergone
575 surface modification by human activity, deposition in closed depressions, or colluvial
576 deposition from adjacent hillslopes. Three samples (DS303-305) that we collected from
577 boulders near the southern limit of the deposit have exposure ages that overlap within
578 uncertainties, and yield an average age of 8.4 ± 0.5 ka.

579 **Summary landslide deposits**

580 Our exposure ages from boulders on the landslide deposits define three age
581 populations (Fig. 15). The oldest population yields an age of $\sim 8-9$ ka and refers to the
582 lowermost landslide deposit. Given our simplifying assumption of negligible erosion of
583 the boulder surfaces, this is likely a minimum age. Because this deposit is unrelated to the
584 adjacent, but topographically lower, $\sim 0.5-1$ ka old Alpine Canyon landslide deposit, we
585 suggest that it represents a remnant of the initial Crystal Lake landslide, which would
586 have extended farther downstream than it does today. Gentle-sloping hillslopes at ~ 1500
587 m elevation, west of the Coldbrook Creek (Fig. 11), could indicate a formerly continuous
588 surface that connected the upper level of the Crystal Lake landslide with the lowermost
589 deposit (Fig. 16). We interpret the $\sim 4-5$ ka old boulders on the upper part of the Crystal
590 Lake landslide as representing another landslide event that could have occurred either
591 independently (cf., Morton et al., 1989), or, as a secondary failure, within the deposits of

592 the initial landslide. Fresh landslide deposits typically display hummocky topography
593 where surface waters can accumulate in local depressions and facilitate secondary slope
594 failures by exerting hydrostatic pressure on the surrounding materials. The slump that
595 borders the higher part of the Crystal Lake landslide could represent such a process at
596 small spatial scale.

597

598 **DISCUSSION**

599 Our results bring new data to bear on deep-seated landsliding, fill terraces, and a
600 potential connection between the two in the North Fork San Gabriel Canyon. First, we
601 evaluate the hypothesis of Bull (1991) that the fill terraces are a result of climate-change-
602 induced changes in sediment supply. Second, we discuss our preferred interpretation that
603 the fill terraces are a result of increased sediment supply and debris-flow activity
604 following deep-seated landslides. Third, we discuss the timing of deep-seated landsliding
605 and potential triggers. Fourth, we discuss the implications of our findings for landscape
606 evolution in the San Gabriel Mountains and for how rapidly-eroding landscapes respond
607 to climate change.

608 **Fill terrace formation caused by climate change?**

609 Bull (1991) argues that valley aggradation in the North Fork San Gabriel Canyon
610 (and elsewhere in the San Gabriel Mountains) was due to climatic changes that caused an
611 increase of hillslope sediment supply relative to the transport capacity of rivers. Although
612 Bull (1991) essentially applies the climate change model to all terraces in the North Fork
613 San Gabriel, he focuses on the T7 terraces, which is also the focus in our study. In this
614 model, the principle mechanism of valley aggradation is fluvial deposition of bedload,
615 which we find difficult to reconcile with our observations. First, there is no record of a
616 major climate shift over the last 7 kyr. Instead, reports of paleoclimatic conditions in
617 southern California during the early Holocene are diverse. For example, Owen et al.
618 (2003) and Kirby et al. (2007) find indications that the early Holocene may have been a
619 time of higher rainfall than today; whereas periods of dune activity and paleolakes in the
620 Mojave Desert suggest that the entire Holocene was comparatively drier than the latest
621 Pleistocene, including the Last Glacial Maximum (Tchakerian and Lancaster, 2002).

622 Furthermore, the Holocene aggradation episode in the North Fork San Gabriel Canyon is
623 concurrent with a period of downcutting from ~10-2 ka in the Cajon Creek area that
624 followed extensive aggradation between 16 and 10 ka (Weldon and Sieh, 1985). Studies
625 from other places around the Western Transverse Ranges indicate that one or several
626 major pulses of aggradation and alluvial fan formation occurred between approximately
627 60 and 30 ka (Weldon and Sieh, 1985; Matmon et al., 2005; Van der Woerd et al., 2006;
628 Fletcher et al., 2010; Behr et al., 2010; McGill et al., 2013; Owen et al., 2014).

629 Second, the spatial confinement of fill terraces to the North Fork San Gabriel
630 Canyon is at odds with climatic forcing and gradual deposition by rivers that ought to
631 have a more regional impact on the drainage network. One explanation could be that the
632 rate of incision into the valley fill had been limited by the epigenetic gorge in the lower
633 part of the North Fork San Gabriel Canyon (Fig. 2) and thereby allowed preservation of
634 much of the valley fill, which was more rapidly eroded in neighboring canyons like that
635 of Bear Creek. This scenario, however, does not explain why fill terraces are absent from
636 the Bichota Canyon because it is a tributary to the North Fork San Gabriel Canyon and
637 should have responded in a similar way. This suggests an evenly distributed valley fill
638 has never existed to the same extent as in the North Fork San Gabriel Canyon, perhaps
639 because very rapid deposition and incision of the valley fill in the North Fork San Gabriel
640 Canyon prevented significant backfilling.

641 Third, the materials that make up the terrace deposits do not have a clear fluvial
642 signature. The lack of sorting, the mostly sub-angular clasts without any discernible
643 imbrication, a matrix-supported texture, the lack of fine scale lamination, and the high
644 amount of sandy to granular matrix material are more typical of debris flow deposits. The
645 high slopes (0.05-0.1) of the present-day river channel, the terrace surfaces, and the
646 stratification within the valley fill, are indeed consistent with slopes reported from debris
647 flow channels (Stock and Dietrich, 2003), and support our observations of debris-flow
648 levees and snouts (e.g., Whipple and Dunne, 1992) across the modern valley floor.
649 Furthermore, the dominance of grains in our terrace sediment samples, whose
650 luminescence signals have not been reset during transport, is consistent with debris flow
651 transport in which grains are only rarely exposed to sunlight. The periodical occurring
652 lenses within the terrace deposits are likely deposits from successive debris flows or

653 surges, or may represent lateral heterogeneity as the main debris-flow lobes shifted across
654 the floodplain (as is apparent in the modern floodplain). Bull (1991), in contrast,
655 interprets the angularity of the T7 deposits as derived from frost weathering of bedrock
656 during full-glacial conditions, but that their transport to the streambed by runoff did not
657 occur until the early- to mid-Holocene. This model requires stable hillslopes over several
658 thousand years during the late Pleistocene and early Holocene (Bull, 1991), which we
659 find hard to reconcile with erosion rates of ~1 mm/yr (DiBiase et al., 2010) in this part of
660 the San Gabriel Mountains.

661 Fourth, we do not observe any significant change in channel slope or grain size
662 between the terrace treads and the modern channel, suggesting no major changes in the
663 transport regime. Grain size distributions within terraces are similar to those in the active
664 channels and floodplains at very different locations within the drainage, which suggests
665 that the processes transporting sediment through the Canyons have remained
666 approximately the same. Although this argument needs to be substantiated with more
667 observations, it would corroborate the hypothesis of a debris-flow origin of both the
668 terrace and the streambed sediments.

669 Finally, because large parts of the San Gabriel Mountains are mostly bedrock with
670 little hillslope storage of sediment, it is unlikely for small changes in climate to cause
671 large changes in sediment supply. Most debris flows in the San Gabriel Mountains are
672 associated with winter storm events and are particularly common after wildfires (e.g.,
673 Doehring, 1968; Lavé and Burbank, 2004; Cannon et al., 2010; Lamb et al., 2011; Kean
674 et al., 2011). There exist numerous historical examples of debris flows that reached urban
675 areas outside of the San Gabriel Mountains (e.g., Chawner, 1935; Morton and Hauser,
676 2001), and these events were the reason for the construction of debris retention basins
677 fringing the San Gabriel Mountains (L.A.C.D.P.W., 1991). According to current models,
678 loose sediments are stored on steep hillslopes behind vegetation dams (Lamb et al., 2011;
679 2013). These are frequently destroyed by wildfires, which have recurrence intervals of
680 ~30 years (DiBiase and Lamb, 2013), and which release the sediment to steep river
681 channels. Ensuing runoff during winter storms evacuates these channels, typically leading
682 to mud and debris flows (Doehring, 1968; Morton and Hauser, 2001; Cannon et al., 2008;
683 Prancevic et al., 2014). The volume of material that can be released from hillslopes is

684 thus limited by the rate of soil production and the size of vegetation dams. Because soil
685 production rates in the San Gabriel Mountains are high (Heimsath et al., 2012), and
686 vegetation dams are rather small, hillslope storage in the San Gabriel Mountains tends to
687 be saturated within decades (Lamb et al., 2011; DiBiase and Lamb, 2013). Therefore, the
688 amount of hillslope material that can be released by environmental changes is strongly
689 limited. Unlike soil-mantled landscapes, in the San Gabriel Mountains there simply is not
690 a large reservoir of colluvium to mine. Moreover, changes in the rate of soil production
691 are likely too small to explain rapid valley aggradation in a few thousand years.

692 At odds with our bedrock-landscape hypothesis is that Bull (1991) suggested that
693 different terraces levels in the North Fork San Gabriel Canyon, in addition to T7, also
694 reflect the impacts of earlier climatic changes. Specifically, the higher lying T1, T3, and
695 T4 terraces (Fig. 5, Fig. 8), were thought to stem from aggradation-incision cycles during
696 the middle to late Pleistocene (Bull, 1991). The abundance of sediment-mantled strath
697 terraces in the Bear Creek Canyon and the West Fork of the San Gabriel River at similar
698 elevations above the river suggests the possibility that these terraces could have a similar
699 origin. Strath terraces are common in the San Gabriel Mountains, and may record an
700 increase in tectonic activity (DiBiase et al., 2014). Unfortunately, we were not able to
701 locate exposures of these terraces to verify if they are fill or strath. While the existence of
702 a T3 terrace is debatable, Bull (1991) observed that the T4 within the North Fork is
703 indeed a fill terrace. Thus, the climate-change hypothesis remains a viable explanation for
704 older terraces in the North Fork San Gabriel River, which deserve targeted future work.

705 **Fill terrace formation caused by deep-seated landslides.**

706 Instead of climate change, here we propose that the deep-seated landslides in the
707 upper part of the North Fork San Gabriel Canyon provided the sediment supply that led
708 to valley aggradation, primarily by debris flows, and the formation of terraces. Fig.
709 **17Error! Reference source not found.** provides a simple sketch of how we think the
710 valley aggradation is related to the deep-seated landslide: (A) First, a more extensive
711 Crystal Lake landslide deposited large amounts of easily erodible material in the
712 headwaters of the North Fork San Gabriel Canyon, probably at around ~8-9 ka. (B, C)
713 Headward erosion into the landslide deposits triggered abundant debris flows that stacked

714 on top of each other and filled up the valley below the landslide, probably at very high
715 rates. (C) Progressive valley aggradation and erosion of the landslide deposits reduces the
716 relief contrasts and the sediment supply, which eventually causes re-incision of the valley
717 fill. In the following paragraphs, we discuss whether this model is consistent with the
718 available data.

719 The landslide deposits in the upper part of the North Fork San Gabriel Canyon
720 constitute a huge storage of unconsolidated material that could account for a long-lived
721 source of debris flows. The Wright Mountain landslide (near the town of Wrightwood,
722 approximately 20 km to the east), for example, formed prior to 1500 AD, but is still an
723 ongoing source of debris flows that are frequently triggered by snowmelt and rain (e.g.,
724 Morton et al., 1979). Following the landslide events in the North Fork San Gabriel
725 Canyon, loose sediments without any vegetation cover were exposed to erosion over
726 large areas of the catchment. Subsequent incision of rivers and debris flows into the
727 landslide deposits has probably been rapid, which is supported by the 35 m of incision
728 into the surface of the Alpine Creek landslide in Clouburst Canyon at an average rate of
729 $\sim 35 \text{ mm yr}^{-1}$ during the last $\sim 1,000$ years. Even nowadays, the headscarp area of the
730 Alpine Creek landslide is feeding large talus cones at rates that are high enough to
731 prevent colonization by vegetation. Once the landslide surface had been colonized by
732 vegetation, the same principles as on other hillslopes apply, namely that wildfires and
733 heavy precipitation events increase the chance for debris flows, only that the supply of
734 loose sediments is not limited by soil production in between wildfires (e.g., Lamb et al.,
735 2011).

736 In case the initial, more extensive Crystal Lake landslide deposit was truly the
737 source of debris flows that built up the valley fill, our estimated volume of the valley fill
738 would have to be smaller than the landslide deposit. Morton et al. (1989) suggested that
739 the Crystal Lake landslide deposit comprises a minimum volume of 0.6 km^3 , but it is not
740 clear what this estimate is based on. Using a landslide area-volume scaling relationship
741 that is based on a global data set ($\text{Volume} = 0.146 \pm 0.005 \times \text{Area}^{1.332 \pm 0.005}$; Larsen et al.,
742 2010), and the currently exposed area of the Crystal Lake landslide ($\sim 7 \text{ km}^2$), we estimate
743 a volume of $1.95 \pm 0.09 \text{ km}^3$. When adding the area of the lowermost landslide deposit
744 (0.4 km^2), near the toe of the Alpine Canyon landslide, the volume estimate increases to

745 2.1±0.09 km³. Therefore, the estimated volume of the valley fill (0.1 km³) could indeed
746 account for the sediments that were eroded from an initial, more extensive Crystal Lake
747 landslide deposit. For comparison, if the entire valley fill were derived from hillslopes
748 upstream of the fill, the equivalent soil/regolith thickness would have to be ~4 m,
749 assuming similar densities. Although this number would be somewhat smaller if part of
750 the valley fill would stem from older aggradation episodes, soils in the San Gabriel
751 Mountains, if present, have typical depths of less than ~75 cm (Dixon et al., 2012;
752 Heimsath et al., 2012). A hillslope origin of the valley fill would thus require
753 significantly thicker soils in the past, which is difficult to reconcile with the high
754 steepness of the hillslope angles (DiBiase and Lamb, 2013).

755 Furthermore, if our hypothesis about the origin of the valley fill in the North Fork
756 San Gabriel Canyon were true, the landslide would have to predate the aggradation of the
757 valley fill. Although we obtained only four IRSL sample ages from the aggradational
758 period, these ages are in good agreement with the two ¹⁴C ages previously obtained by
759 Bull (1991), and suggest that between 7 and 8 ka, aggradation of the valley fill was
760 underway. Because the base of the valley fill is currently not exposed, the aggradation
761 phase likely initiated somewhat earlier, but it is difficult to judge by how much. From
762 measurements of sediment yield of the San Gabriel River, we can estimate the timescale
763 for depositing the valley fill. Between 1937 and 2006, the mean annual sediment
764 accumulation behind the San Gabriel Dam was ~580,000 m³ yr⁻¹ (L.A.C.D.P.W., 1991),
765 which is equivalent to a mean basin-wide erosion rate in the San Gabriel catchment of ~1
766 mm yr⁻¹, consistent with cosmogenic exposure-age dating in the region (DiBiase et al.,
767 2010). The annual sediment yield from areas upstream of the valley fill (~25 km²),
768 amounts to approximately 25,000 m³ yr⁻¹, and filling up the valley with ~0.1 km³ of
769 sediment would thus have taken approximately 4,000 years. These sediment yields,
770 however, correspond to areas that are largely free of landslide material and it is most
771 likely that sediment yields from the landslide areas have been much higher, resulting in
772 more rapid valley aggradation.

773 It has been shown previously that sediment yields from recently burned areas are
774 often an order of magnitude higher than the background rates, presumably due to the
775 transition from supply- to transport-limited processes (Doehring, 1968; Lavé and

776 Burbank, 2004; Lamb et al., 2011). If the same logic applies to fresh landslide deposits
777 where loose sediment is virtually unlimited, the filling could potential occur over a few
778 hundred years. The apparent rapid incision of the Alpine Canyon landslide and the lack
779 of aggradation in Bichota Canyon support our assumption that the landslide material is
780 easier to erode than bedrock. Decadal hillslope erosion rates in the Illgraben, one of the
781 most active debris-flow catchment in the Swiss Alps (Schlunegger et al., 2009), for
782 example, range between ~ 200 and 400 mm yr^{-1} (Bennett et al., 2012, 2013). Although
783 this catchment contains no large landslide deposit, it is developed in highly fractured
784 metasedimentary rocks that might be considered comparable. Korup et al. (2004)
785 estimated immediate post-failure sediment yields from three large historic landslides in
786 the Southern Alps, New Zealand, to be in excess of $70,000 \text{ t km}^{-2} \text{ yr}^{-1}$, which translates to
787 erosion rates of $\sim 37 \text{ mm yr}^{-1}$ (for an assumed landslide deposit density of 1.9 g cm^{-3}).
788 Decadal scale erosion rates were on the order of $13\text{-}18 \text{ mm yr}^{-1}$ and resulted in rapid
789 valley aggradation over a downstream length of $>7.5 \text{ km}$ (Korup et al., 2004). From these
790 numbers, and our millennial incision rate of the Alpine Canyon landslide deposit, erosion
791 rates of landslide deposits in the North Fork San Gabriel Canyon of $>10 \text{ mm yr}^{-1}$ appear
792 plausible and would allow filling up the valley in less that $\sim 650\text{-}800$ years, for typical
793 trapping efficiencies of $\sim 50\text{-}60\%$ (Korup et al., 2004). Therefore, we conclude that the
794 time frame for valley aggradation postdating the earliest landslide ($\sim 8\text{-}9 \text{ ka}$) in the North
795 Fork San Gabriel Canyon appears to be reasonable.

796 In our study we did not constrain the age of the T7 terrace surface, which we
797 consider the top surface of the post-landslide valley fill. If valley aggradation was truly
798 rapid, re-incision of the valley fill might have started soon after $\sim 7 \text{ ka}$, probably at a rate
799 that is limited by bedrock incision in the epigenetic gorge. During the downcutting, the
800 formation of multiple cut-terraces could occur even in the absence of climatic changes
801 (Limaye and Lamb, 2014; in review). In this regard, one may wonder if the older
802 terraces, i.e., T1, T4, and perhaps T3, could have been formed in a similar fashion. At this
803 stage, there do not exist enough observations to conclude, but the $\sim 33\text{-ka}$ boulder age we
804 obtained from near the drainage divide with the Bear Creek may indicate an even older
805 landslide, which could have triggered a similar episode of aggradation and incision that
806 produced the older terraces. It is also possible that these terraces represent cuts into the

807 same landslide-derived fill as the younger ones. The more extensive planation of the T7
808 surface could then be related to a change in substratum when the river encountered
809 bedrock and formed the epigenetic gorge. Finally, the T1 and T4 terraces could also be
810 strath terraces similar to the ones we observe in the Bear Creek, but according to Bull
811 (1991), at least the T4 terrace consists of alluvium.

812 **Landslide trigger and timing**

813 There exist abundant landslide deposits within the San Gabriel Mountains
814 (Morton and Miller, 2006), but the Crystal Lake and Alpine Canyon landslides in the
815 North Fork San Gabriel Canyon are the most extensive ones (Morton et al., 1989). An
816 obvious question is therefore if they owe their occurrence to special conditions
817 exclusively found in this valley? Neither the present-day local climate, nor the bedrock
818 geology, or the proximity to active faults like the San Andreas Fault, appears sufficiently
819 distinct from the rest of the San Gabriel Mountains to favor large landslides exclusively
820 in the North Fork San Gabriel Canyon. The gentle-sloping terrain in the vicinity of the
821 San Gabriel Fault Zone (Fig. 2) suggests that tectonically induced fractures act to lower
822 rock mass strength but there is no obvious fault zone in the upper part of the North Fork
823 San Gabriel Canyon. We note however, that this canyon lies within a zone of very high
824 relief that stretches from the Bear Creek Canyon eastwards across the North Fork San
825 Gabriel Canyon and the Mount Baldy area towards the southeastern edge of the San
826 Gabriel Mountains (Fig. 18). Regions that lie to the northwest of the North Fork San
827 Gabriel and Bear Creek Canyons are relatively high in altitude (>1500 m), but exhibit
828 lower relief. Cosmogenic-nuclide derived erosion rates (DiBiase et al., 2010) and mineral
829 cooling ages (Blythe et al., 2000) record much faster short- and long-term erosion of the
830 high relief versus the low-relief areas, which implies that headward incision of the San
831 Gabriel drainage maintains or accentuates the relief contrast between these two
832 morphologic domains. As a result, topographically induced stresses in the high-relief area
833 are likely larger than in regions of lower relief (e.g., Miller and Dunne, 1996). It is clear
834 that the Crystal Lake and Alpine Creek landslide deposits have reduced the topographic
835 relief in the headwaters of the North Fork San Gabriel Canyon. In fact, the present-day
836 topography in the headwaters of the Bear Creek Canyon may resemble that of the North

837 Fork San Gabriel Canyon prior to failure. Consequently, the headwaters of Bear Creek
838 Canyon could potentially be sites of future large landslides. It is also conceivable that
839 similar large landslides, of which no more evidence exists, occurred during earlier times
840 in areas of rapid valley incision and high topographic relief.

841 Periods of wetter climates may trigger large landslides through enhanced pore
842 pressure (e.g., Bookhagen et al., 2005; Dortch et al., 2009; Zerathe et al., 2014). Because
843 past climatic changes in the San Gabriel Mountains are debated, it remains uncertain if
844 they could have affected the timing of landslides in the North Fork San Gabriel Canyon.
845 However, irrespective of potential climatic influences, the proximity of the San Gabriel
846 Mountains to seismogenic faults seems to provide ample opportunities to trigger large
847 slope failures on a frequent basis. Palaeoseismic records from Wrightwood indicate
848 recurrence intervals of surface rupturing earthquakes along the San Andreas Fault of
849 ~100 years over the past 1500 years (Weldon et al., 2004). Although recurrence interval
850 estimates for other seismogenic faults, like the Sierra Madre-Cucamonga Fault Zone to
851 the south (Fig. 1A) do not exist, historical ruptures (Lindvall and Rubin, 2008) show their
852 potential for ground acceleration. Hence, we suspect that the topographic conditions in
853 the headwaters of the North Fork San Gabriel Canyon were the primary factors for the
854 occurrence of exceptionally large landslides, while seismic shaking may have been the
855 actual trigger.

856 **Implications for landscape evolution in the San Gabriel Mountains**

857 Our study has shown that the North Fork San Gabriel Canyon has been in a state
858 of topographic disequilibrium since at least ~8-9 ka. The lower part of the North Fork
859 San Gabriel Canyon may have been filled with sediments by ~6-7 ka, followed by
860 incision. The fact that likely >60% of the valley fill has not yet been excavated, suggests
861 that it may take another ~10 thousand years before the North Fork San Gabriel River
862 reaches bedrock again, probably regulated by the rate of river incision within the
863 epigenetic gorge near the confluence with the West Fork of the San Gabriel River.
864 Although incision into the landslide deposits appears to proceed very rapidly, the sheer
865 volume of the landslide deposit is sufficient to keep the upper part of the North Fork San
866 Gabriel Canyon in a transient state for many thousand years to come. This circumstance

867 may also explain part of the scatter that is seen in functional relationships between
868 topographic metrics, such as channel steepness or local relief, and rates of erosion
869 estimated from thermochronology (Spotila et al., 2002) or cosmogenic nuclides (DiBiase
870 et al., 2010).

871 There exist other catchments in the San Gabriel Mountains where debris flows
872 frequently occur and where the valley has been buried by considerable amounts of
873 sediments (Fig. 19). Examples include active debris-flow catchments on the southwestern
874 slope of Mount Baldy (Fig. 19A), or to the east of Mt. Baden-Powell (Fig. 19B). There
875 also exist catchments where deposits with debris-flow channels on the surface provide
876 evidence for past debris-flow activity (Fig. 19C). A tributary of the Big Tujunga River
877 features voluminous deposits that have already been incised again (Fig. 19D). Similar to
878 the North Fork San Gabriel Canyon, these fill deposits are in contrast to widespread
879 strath terraces in the main stem of the Big Tujunga Canyon (DiBiase et al., 2014). The
880 above examples indicate that valley aggradation by debris flows may in fact be a frequent
881 process that affects higher-order drainages in the San Gabriel Mountains, and provide
882 another indication of topographic and erosional disequilibrium.

883 **Implications for climate change impacts in rapidly-eroding bedrock landscapes**

884 Our study has shown that concepts of how hillslopes and rivers respond to climate
885 change that are largely based on landscapes with thick soil mantles (e.g., Bull, 1991) may
886 not apply to steep, and rapidly-eroding arid bedrock landscapes. Although river terraces
887 have proven to be useful indicators of climate change in glaciated and soil-mantled
888 landscapes (e.g., Knox, 1983; Bull, 1991; Bridgland and Westaway, 2008; Pazzaglia,
889 2013), there currently exists little evidence that they form in a similar fashion in the San
890 Gabriel Mountains. We think that this is partly related to the limited amount of hillslope
891 sediment that can be stored in these environments. Although prolonged periods of more
892 humid conditions could allow for changing the type of vegetation cover and therefore the
893 damming capacities, this only leads to increasing hillslope storage if wildfires do not
894 destroy these dams on a regular basis as they do now, and if soil production rates are
895 higher than river incision rates. Heimsath et al. (2012) reported soil production rates in
896 the San Gabriel Mountains of up to $\sim 0.5 \text{ mm yr}^{-1}$, but rates higher than $\sim 0.2 \text{ mm yr}^{-1}$ only

897 occur on hillslopes steeper than 30°, with thin (<30 cm) and patchy soil cover that is
898 frequently stripped off by landslides (Heimsath et al., 2012; DiBiase et al., 2012).

899 Although soil production rates may increase with precipitation, observations
900 indicate that this holds only for low erosion rates (<0.05 mm yr⁻¹; Dere et al., 2013) and
901 is more pronounced under arid to hyperarid conditions (mean annual precipitation <100
902 mm yr⁻¹; Owen et al., 2011). Therefore, even if climatic changes in the San Gabriel
903 Mountains would cause markedly more humid conditions, the ability to accumulate
904 significant amounts of sediment on hillslopes appears limited, mainly because they are
905 rapidly uplifting and steeper than the angle of repose (e.g., Lamb et al., 2011; DiBiase et
906 al., 2012). A fundamental transition from bedrock to soil-covered hillslopes would thus
907 require lower hillslope angles. However, erosion rates from decades to thousands of years
908 and millions of years show no major changes (Blythe et al., 2000; Spotila et al., 2002;
909 Lavé and Burbank, 2004; DiBiase et al., 2010; Lamb et al., 2011), and landscape
910 adjustment timescales to changes in uplift rate in the San Gabriel Mountains play out over
911 a few million years (DiBiase et al., 2014).

912 Loose sediment may also accumulate in colluvial hollows before it enters the
913 valley network (e.g., Reneau et al., 1990). However, in the San Gabriel Mountains,
914 colluvial hollows are typically scoured by debris flows that are frequently triggered by
915 winter storms and are particularly common after wildfires (e.g., Kean et al., 2011).
916 Furthermore, our work and previous studies (Stock and Dietrich, 2003, 2006) suggest that
917 considerable parts of the San Gabriel Mountains are shaped by debris flows, and it is also
918 not clear how debris flow channels respond to changes in sediment supply and water
919 discharge. Together, these unknowns make it difficult to determine the response of steep,
920 unglaciated bedrock landscapes to climate change. It is clear, however, that lessons
921 learned from glaciated, fluvial-dominated, and soil-mantled landscapes may not simply
922 translate to steep bedrock landscapes.

923 **CONCLUSION**

924 The North Fork San Gabriel Canyon is an arid, rapidly eroding, bedrock
925 landscape in the San Gabriel Mountains, CA, which features a series of prominent fill
926 terraces that were previously related to periods of river aggradation induced by climatic

927 changes (Bull, 1991). We challenge this view and instead propose that deep-seated
928 landslides in the upper part of the North Fork San Gabriel Canyon provided voluminous
929 sediment supply that led to valley aggradation, primarily by debris flows, and the
930 formation of terraces. A debris flow origin of the terrace deposits is supported by our
931 morphological and sedimentological observations, the scarcity of grains that were
932 exposed to sunlight long enough to completely bleach their luminescence signal, and is
933 consistent with abundant debris flow deposits throughout the San Gabriel Mountains. Our
934 new Holocene exposure ages reveal that the Crystal Lake and Alpine Canyon landslides
935 are much younger than previously assumed, and that subsequent erosion of the landslide
936 material was very rapid. The debris flow origin of the terrace deposits renders accurate
937 dating of the aggradation period by luminescence methods difficult, but our new ages
938 based on post-IR IRSL single grain dating are consistent with available ^{14}C ages, and
939 indicate that aggradation occurred during the early-mid Holocene, subsequent to the
940 oldest landslide event. The occurrence of these landslides in the North Fork San Gabriel
941 Canyon is probably promoted by large topographic stresses and deep weathering of the
942 pre-uplift topography.

943 These results show that enhanced sediment supply following large deep-seated
944 landslides can produce valley fills and terraces that resemble fluvial terraces, especially
945 when the debris flow deposits are fluvial reworked, but may have origins independent of
946 climate change. In fact, the lack of a continuous soil cover and the limited storage of
947 hillslope sediments in steep and arid bedrock landscapes appears to greatly limit the
948 potential for climatic changes to cause significant valley aggradation by fluvial
949 deposition. Furthermore, our study has shown that erosion and sediment transport
950 processes in the San Gabriel Mountains can be highly episodic in space and time, and
951 interspersed with aggradational periods. These circumstances create ambiguity in the
952 interpretation of erosion rate estimates that integrate over timescales of less than 10^4
953 years and relationships between landscape-scale erosion rates and morphometric
954 parameters.

955

956 **ACKNOWLEDGEMENTS**

957 This project was supported by the Gordon and Betty Moore Foundation, through
958 the Tectonics Observatory, NSF grant EAR0838495. D.S. was supported by a Feodor
959 Lynen Scholarship through the Alexander von Humboldt Foundation. M.P.L.
960 acknowledges support from the donors of the American Chemical Society Petroleum
961 Research Fund. This work started as a Caltech class project, and we are thankful for help
962 from the participants of Ge125.

963

964 **REFERENCES CITED**

- 965 Armitage, J.J., Duller, R.A., Whittaker, A.C., and Allen, P.A., 2011, Transformation of tectonic and
966 climatic signals from source to sedimentary archive: *Nature Geoscience*, v. 4, p. 231-235,
967 doi:10.1038/NGEO108.
- 968 Balco, G., Stone, J., Lifton, N., and Dunai, T., 2008, A complete and easily accessible means of calculating
969 surface exposure ages or erosion rates from ^{10}Be and ^{26}Al measurements: *Quaternary*
970 *Geochronology*, v. 3, p. 174-195, doi:10.1016/j.quageo.2007.12.001.
- 971 Behr, W.M., Rood, D.H., Fletcher, K.E., Guzman, N., Finkel, R., Hanks, T.C., Hudnut, K.W., Kendrick,
972 K.J., Platt, J.P., Sharp, W.D., Weldon, R.J., and Yule, J.D., 2010, Uncertainties in slip-rate
973 estimates for the Mission Creek strand of the southern San Andreas fault at Biskra Palms Oasis,
974 Southern California: *Geological Society of America Bulletin*, v. 122, p. 1360-1377.
- 975 Bennett, G.L., Molnar, P., Eisenbeiss, H., and McArdell, B.W., 2012, Erosional power in the Swiss Alps:
976 characterization of slope failure in the Illgraben: *Earth Surface Processes and Landforms*, v. 37, p.
977 1627-1640.
- 978 Bennett, G.L., Molnar, P., McArdell, B.W., Schlunegger, F., and Burlando, P., 2013, Patterns and controls
979 of sediment production, transfer and yield in the Illgraben: *Geomorphology*, v. 188, p. 68-82.
- 980 Blum, M.D., and Törnqvist, T.E., 2000, Fluvial responses to climate and sea-level change: a review and
981 look forward: *Sedimentology*, v. 47, p. 2-48.
- 982 Blythe, A.E., Burbank, D.W., Farley, K.A., and Fielding, E.J., 2000, Structural and topographic evolution
983 of the central Transverse Ranges, California, from apatite fission-track, (U-Th)/He and digital
984 elevation model analyses: *Basin Research*, v. 12, p. 97-114.
- 985 Blythe, A.E., House, M.A., and Spotila, J.A., 2002, Low-temperature thermochronology of the San Gabriel
986 and San Bernadino Mountains, southern California: Constraining structural evolution, in Barth, A.,
987 ed., *Contributions to Crustal Evolution of the Southwestern United States*: Boulder, Colorado,
988 Geological Society of America Special Paper, v. 365, p. 231-250.
- 989 Bookhagen, B., Thiede, R.C., and Strecker, M.R., 2005, Late Quaternary intensified monsoon phases
990 control landscape evolution in the northwest Himalaya: *Geology*, v. 33, no. 2, p. 149-152.

991 Brakenridge, G.R., 1980, Widespread episodes of stream erosion during the Holocene and their climatic
992 cause: *Nature*, v. 283, p. 655-656.

993 Bridgland, D., and Westaway, R., 2008, Climatically controlled river terrace staircases: A worldwide
994 Quaternary phenomenon: *Quaternary Science Reviews*, v. 98, p. 285-315.

995 Bull, W.B., 1979, Threshold of critical power of streams: *Geological Society of America Bulletin*, v. 90, p.
996 453-464.

997 Bull, W.B., 1991, *Geomorphic responses to climatic change*: Oxford University Press, New York.

998 Buylaert, J.P., Murray, A.S., Thomsen, K.J., and Jain, M., 2009, Testing the potential of an elevated
999 temperature IRSL signal from K-feldspar: *Radiation Measurements*, v. 44, p. 560-565.

1000 Cannon, S.H., Boldt, E.M., Kean, J.W., Laber, J.L., Staley, D.M., 2010, Relations Between Rainfall and
1001 Postfire Debris-Flow and Flood Magnitudes for Emergency-Response Planning, San Gabriel
1002 Mountains, Southern California: USGS Open-File Report 2010-1039.

1003 Cannon, S.H., Gartner, J.E., Wilson, R.C., Bowers, J.C., and Laber, J.L., 2008, Storm rainfall conditions
1004 for floods and debris flows from recently burned areas in southwestern Colorado and southern
1005 California: *Geomorphology*, v. 96, p. 250-269.

1006 Chawner, W.D., 1935, Alluvial fan flooding: The Montrose, California, flood of 1934: *Geographical*
1007 *Review*, v. 25, p. 255-263.

1008 Crook, R. Jr., 1986, Relative dating of Quaternary deposits based on P-Wave velocities in weathered
1009 granitic clasts: *Quaternary Research*, v. 25, p. 281-292.

1010 Davis, W.M., 1909, *Geographical Essays*: Dover Publications, 777 p.

1011 Dere, A.L., White, T.S., April, R.H., Reynolds, B., Miller, T.E., Knapp, E.P., McKay, L.D., and Brantles,
1012 S.L., 2013, Climate dependence of feldspar weathering in shale soils along a latitudinal gradient:
1013 *Geochimica et Cosmochimica Acta*, v. 122, p. 101-126, doi: 10.1016/j.gca.2013.08.001.

1014 DiBiase, R.A., Whipple, K.X., Lamb, M.P., Heimsath, A.M., 2014, The role of waterfalls and knickzones
1015 in controlling the style and pace of landscape adjustment in the western San Gabriel Mountains,
1016 California: *Geological Society of America Bulletin*, v. 127, p. 539-559, doi: 10.1130/B31113.1.

1017 DiBiase, R.A., 2011, *Tectonic Geomorphology of the San Gabriel Mountains, CA [PhD Thesis]*: Tempe,
1018 Arizona State University, 247 p.

1019 DiBiase, R.A., and Lamb, M.P., 2013, Vegetation and wildfire controls on sediment yield in bedrock
1020 landscapes: *Geophysical Research Letters*, v. 40, p. 1-5, doi:10.1029/2013GL055108.

1021 DiBiase, R.A., and Whipple, K.X., 2011, The influence of erosion thresholds and runoff variability on the
1022 relationships among topography, climate, and erosion rate: *Journal of Geophysical Research*, v.
1023 116, F04036, doi:10.1029/2011JF002095.

1024 DiBiase, R.A., Whipple, K.X., Heimsath, A.M., and Ouimet, W.B., 2010, Landscape form and millennial
1025 erosion rates in the San Gabriel Mountains, CA: *Earth and Planetary Science Letters*, v. 289(1-2),
1026 p. 134-144, doi:10.1016/j.epsl.2009.10.036.

1027 DiBiase, R.A., Heimsath, A.M., and Whipple, K.X., 2012, Hillslope response to tectonic forcing in
1028 threshold landscapes: *Earth Surf. Process. Landforms*, v. 37, p. 855–865, doi: 10.1002/esp.3205.

1029 Dixon, J.L., Hartshorn, A.S., Heimsath, A.M., DiBiase, R.A., and Whipple, K.X., 2012, Chemical
1030 weathering response to tectonic forcing: A soils perspective from the San Gabriel Mountains,
1031 California: *Earth and Planetary Science Letters*, v. 323-324, p. 40-49.

1032 Doehring, D.O., 1968, The effect of fire on geomorphic processes in the San Gabriel Mountains,
1033 California: *Wyoming Univ. Contr. Geology*, v. 7, p. 43-65.

1034 Dortch, J.M., Owen, L.A., Haneberg, W.C., Caffee, M.C., Dietsch, C., and Kamp, U., 2009, Nature and
1035 timing of large landslides in the Himalaya and Transhimalaya of northern India: *Quaternary
1036 Science Reviews*, v. 28, p. 1037-1054.

1037 Dunne, J., Elmore, D., and Muzikar, P., 1999, Scaling factors for the rates of production of cosmogenic
1038 nuclides for geometric shielding and attenuation at depth on sloped surfaces: *Geomorphology*, v.
1039 27, p. 3-11.

1040 Eaton, E.C., 1935, Flood and erosion control problems and their solution: *American Society of Civil
1041 Engineers Transactions*, v. 101, p. 1302–1330.

1042 Finnegan, N.J., and Dietrich, W.E., 2011, Episodic bedrock strath terrace formation due to meander
1043 migration and cutoff: *Geology*, v. 39(2), p. 143-146.

1044 Fletcher, K.E.K., Sharp, W.D., Kendrick, K.J., Behr, W.M., Hudnut, K.W., and Hanks, T., 2010, ²³⁰Th/U
1045 dating of a late Pleistocene alluvial fan along the southern San Andreas fault: *Geological Society
1046 of America Bulletin*, v. 122, p. 1347-1359.

1047 Flint, J.J., 1974, Stream gradient as a function of order, magnitude, and discharge: *Water Resources
1048 Research*, v. 10, p. 969– 973.

1049 Hack, J.T., 1957, Studies of longitudinal stream profiles in Virginia and Maryland: U. S. Geological Survey
1050 Professional Papers, 294-B, p. 97.

1051 Heimsath, A.M., DiBiase, R.A., and Whipple, K.X., 2012, Soil production limits and the transition to
1052 bedrock-dominated landscapes: *Nature Geosciences*, v. 5(3), p. 210–214, doi:10.1038/ngeo1380.

1053 Jennings, C.W., and Bryant, W.A., 2010, Fault activity map of California: California Geological Survey
1054 Geologic Data Map No. 6, map scale 1:750,000.

1055 Kean, J.W., Staley, D.M., and Cannon, S.H., 2011, In situ measurements of post-fire debris flows in
1056 southern California: Comparisons of the timing and magnitude of 24 debris-flow events with
1057 rainfall and soil moisture conditions: *Journal of Geophysical Research*, v. 116, F04019,
1058 doi:10.1029/2011jf002005.

1059 Kean, J. W., S. W. McCoy, G. E. Tucker, D. M. Staley, and J. A. Coe, 2013, Runoff-generated debris
1060 flows: Observations and modeling of surge initiation, magnitude, and frequency, *J. Geophys. Res.*
1061 *Earth Surf.*, 118, 2190–2207, doi:10.1002/jgrf.20148.

1062 Kirby, E., and Whipple, K.X., 2012, Expression of active tectonics in erosional landscapes: *Journal of
1063 Structural Geology*, v. 44, p. 54-75.

- 1064 Kirby, M.E., Lund, S.P., Anderson, M.A., Bird, B.W., 2007, Insolation forcing of Holocene climate change
1065 in Southern California: a sediment study from Lake Elsinore: *Journal of Paleolimnology*, v. 38, p.
1066 395-417.
- 1067 Knox, J.C., 1983, Responses of river systems to Holocene climates, In Wright Jr., H.E., ed., *Late*
1068 *Quaternary Environments of the United States*, Vol. 2. *The Holocene*: University of Minnesota
1069 Press, Minneapolis, pp. 26-41.
- 1070 Korup, O., McSaveney, M.J., and Davies, T.R.H., 2004, Sediment generation and delivery from large
1071 historic landslides in the Southern Alps, New Zealand: *Geomorphology*, v. 61, p. 189-207.
- 1072 Korup, O., Strom, A.L., and Weidinger, J.T., 2006, Fluvial response to large rock-slope failures: Examples
1073 from the Himalayas, the Tien Shan, and the Southern Alps in New Zealand: *Geomorphology*, v.
1074 78, p. 3-21.
- 1075 Lal, D., 1991, Cosmic-ray labeling of erosion surfaces: In situ nuclide production-rates and erosion models:
1076 *Earth and Planetary Science Letters*, v. 104(2-4), p. 424-439.
- 1077 Lamb, M.P., Scheingross, J.S., Amidon, W.H., Swanson, E., and Limaye, A., 2011, A model for fire-
1078 induced sediment yield by dry ravel in steep landscapes: *Journal of Geophysical Research*, v. 116,
1079 F03006, doi:10.1029/2010jf001878.
- 1080 Lamb, M.P., Levina, M., DiBiase, R.A., and Fuller, B., 2013, Sediment storage by vegetation in steep
1081 bedrock landscapes: Theory, experiments, and implications for postfire sediment yield: *Journal of*
1082 *Geophysical Research*, v. 118, p. 1147-1160, doi:10.1002/jgrf.20058.
- 1083 Lane, E.W., 1955, The importance of fluvial morphology in hydraulic engineering: *American Society of*
1084 *Civil Engineers Proceedings Separate*, v. 81(745), p. 1-17.
- 1085 Larsen, I.J., Montgomery, D.R., and Korup, O., 2010, Landslide erosion controlled by hillslope material:
1086 *Nature Geoscience*, v. 3, p. 247-251.
- 1087 Lavé, J., and Burbank, D., 2004, Denudation processes and rates in the Transverse Ranges, southern
1088 California: Erosional response of a transitional landscape to external and anthropogenic forcing:
1089 *Journal of Geophysical Research - Earth Surface*, v. 109, F01006, doi:10.1029/2003jf000023.
- 1090 Lavé, J., and Avouac, J.-P., 2001, Fluvial incision and tectonic uplift across the Himalayas of central
1091 Nepal: *Journal of Geophysical Research*, v. 106, no. B12, p. 26,561-26,591.
- 1092 Leopold, L.B., Wolman, M.G., and Miller, J.P., 1964, *Fluvial Processes in Geomorphology*: San Francisco,
1093 W. H. Freeman and Co., 522p.
- 1094 Limaye, A.B.S., and Lamb, M.P., 2014, Numerical simulations of bedrock valley evolution by meandering
1095 rivers with variable bank material: *Journal of Geophysical Research*, v. 119, doi:
1096 10.1002/2013JF002997.
- 1097 Limaye, A.B.S., and Lamb, M.P., Numerical model predictions of autogenic fluvial terraces and
1098 comparison to climate change expectations: in review at *Journal of Geophysical Research –Earth*
1099 *Surface*.

- 1100 Lindvall, S.C., and Rubin, C.M., 2008, Slip rate studies along the Sierra Madre-Cucamonga fault system
1101 using geomorphic and cosmogenic surface exposure age constraints: collaborative research with
1102 Central Washington University and William Lettis & Associates, Inc.: U.S. Geological Survey
1103 final report 03HQGR0084.
- 1104 Los Angeles County Department of Public Works (L.A.C.D.P.W.), 1991, Hydrology Manual, reference
1105 guide, Los Angeles, Calif.
- 1106 Mackin, J.H., 1948, Concept of the graded river: Geological Society of America Bulletin, v. 101, p. 1373-
1107 1388.
- 1108 Matmon, A., Schwartz, D.P., Finkel, R., Clemmens, S., and Hanks, T., 2005, Dating offset fans along the
1109 Mojave section of the San Andreas fault using cosmogenic ²⁶Al and ¹⁰Be: Geological Society of
1110 America Bulletin, v. 117, p. 795-807.
- 1111 Matti, J.C. and Morton, D.M., 1993, Paleogeographic evolution of the San Andreas fault in southern
1112 California: A reconstruction based on a new cross-fault correlation, in Powell, R. E., et al., eds.,
1113 The San Andreas Fault System, Displacement Palinspastic Reconstruction, and Geologic
1114 Evolution: Boulder, Colorado, Geological Society of America Memoir, v. 178, p. 107-
1115 159. McFadden, L.D., and Weldon, R. J., II, 1987, Rates and processes of soil development on
1116 Quaternary terraces in Cajon Pass, California: Geological Society of America Bulletin, v. 98, p.
1117 280-293.
- 1118 McGill, S.F., Owen, L.A., Weldon, R.J., II, and Kendrick, K.J., 2013, Latest Pleistocene and Holocene slip
1119 rate for the San Bernardino strand of the San Andreas fault, Plunge Creek, Southern California:
1120 Implications for strain partitioning within the southern San Andreas fault system for the last ~35
1121 k.y.: Geological Society of America Bulletin, v. 125, p. 48-72.
- 1122 Merritts, D.J., Vincent, K.R., and Wohl, E.E., 1994, Long river profiles, tectonics, and eustasy: A guide to
1123 interpreting fluvial terraces: Journal of Geophysical Research, v. 99, p. 14031-14050.
- 1124 Miller, D.J., and Dunne, T., 1996, Topographic perturbations of regional stresses and consequent bedrock
1125 fracturing: Journal of Geophysical Research, v. 101(B11), p. 25,523-25,536.
- 1126 Miller, W.J., 1926, Glaciation in the San Gabriel Mountains, California: Journal of Geology, v. 34(1), p.
1127 74-82.
- 1128 Molnar, P., Anderson, R.S., Kier, G., and Rose, J., 2006, Relationships among probability distributions of
1129 stream discharges in floods, climate, bed load transport, and river incision: Journal of Geophysical
1130 Research, v. 111, F02001, doi:10.1029/2005JF000310.
- 1131 Montgomery, D.R., Hallet, B., Yüping, L., Finnegan, N., Anders, A., Gillespie, A., and Greenberg, H.M.,
1132 2004, Evidence for Holocene megafloods down the Tsangpo River gorge, southeastern Tibet:
1133 Quaternary Research, v. 62, p. 201-207.
- 1134 Morton, D.M., and Hauser, R.M., 2001, A Debris Avalanche at Forest Falls, San Bernardino County,
1135 California, July 11, 1999: U.S. Geological Survey Open-File Report 2001-146 Version 1.0, 67 p.

1136 Morton, D.M., and Miller, F.K., 2006, Geologic Map of the San Bernardino and Santa Ana 30' x 60'
1137 quadrangles, California: U.S. Geological Survey Open-File Report 2006-1217 Version 1.0.

1138 Morton, D.M., Campbell, R.H., Barrows, A.G., Jr., Kahle, J.E., and Yerkes, R.F., 1979, Part 2: Wright
1139 Mountain mudflows-Spring 1969, in Landsliding and mudflows at Wrightwood, San Bernardino
1140 County, California: California Division of Mines and Geology Special Report, v. 136, p.7-21.

1141 Morton, D.M., Sadler, P.M., and Minnich, R.A., 1989, Large rock-avalanche deposits: examples from the
1142 central and eastern San Gabriel Mountains of Southern California, in Sadler, P.M., and Morton,
1143 D.M., eds., Landslides in a semi-arid environment with emphasis on the Inland Valleys of
1144 Southern California: Publications of the Inland Geological Society, v. 2, p. 323-337.

1145 National Research Council, 2010, Landscapes on the Edge, Washington, The National Academies Press,
1146 180 p.

1147 Nishiizumi, K., Imamura, M., Caffee, M. C., Southon, J. R., Finkel, R. C., and McAninch, J., 2007,
1148 Absolute calibration of ¹⁰Be AMS standards: Nuclear Instruments and Methods in Physics
1149 Research B, v. 258, p. 403-413.

1150 Ouimet, W.B., Whipple, K.X., Crsoby, B.T., Johnson, J.P., and Schildgen, T.F., 2008, Epigenetic gorges in
1151 fluvial landscapes: Earth Surface Processes and Landforms, v. 33, p. 1993-2009.

1152 Owen, J.J., Amundson, R., Dietrich, W.E., Nishiizumi, K., Sutter, B., and Chong, G., 2011, The sensitivity
1153 of hillslope bedrock erosion to precipitation: Earth Surface Processes and Landforms, v. 36, p.
1154 117-135, doi:10.1002/esp.2083.

1155 Owen, L.A., Finkel, R.C., Minnich, R.A., and Perez, A.E., 2003, Extreme southwestern margin of late
1156 Quaternary glaciation in North America: Timing and controls: Geology, v. 31(8), p. 729-732.

1157 Owen, L.A., Clemmens, S.J., Finkel, R.C., and Gray, H., 2014, Late Quaternary alluvial fans at the eastern
1158 end of the San Bernardino Mountains, Southern California: Quaternary Science Reviews, v. 87, p.
1159 114-134.

1160 Parker, G., and Klingeman, P.C., 1982, On why gravel bed streams are paved: Water Resources Research,
1161 vol. 18(5), p. 1409-1423.

1162 Pazzaglia, F.J., and Brandon, M.T., 2001, A fluvial record of long-term steady-state uplift and erosion
1163 across the Cascadia forearc high, western Washington State: American Journal of Science, v. 301,
1164 p. 385-431.

1165 Pazzaglia, F.J., 2013, Fluvial terraces, In Shroder, J., and Wohl, E. (eds.), Treatise on Geomorphology:
1166 Academic Press, San Diego, CA, vol. 9, Fluvial Geomorphology, pp. 379-412.

1167 Perron, J.T., and Royden, L., 2012, An integral approach to bedrock river profile analysis: Earth Surface
1168 Processes and Landforms, v. 38, p. 570-576, doi:10.1002/esp.3302.

1169 Petersen, M.D., and Wesnousky, S. G., 1994, Fault Slip Rates and Earthquake Histories for Active Faults in
1170 Southern California: Bulletin of the Seismological Society of America, v. 84, p. 1608-1649.

1171 Poisson, B., and Avouac, J.-P., 2004, Holocene hydrological changes inferred from alluvial stream
1172 entrenchment in North Tian Shan (northwestern China): *Journal of Geology*, v. 112(2), p. 231-
1173 249.

1174 Porter, S.C., Zhisheng, A., and Hongbo, Z., 1992, Cyclic Quaternary Alluviation and Terracing in a
1175 Nonglaciaded Drainage Basin on the North Flank of the Qinling Shan, Central China: *Quaternary*
1176 *Research*, v. 38, p. 157-169.

1177 Prancevic, J., Lamb, M.P., and Fuller, B., 2014, Initial sediment transport across the river-debris flow
1178 transition: *Geology*, vol. 42(3), p. 191-194, doi: 10.1130/G34927.1

1179 Reneau, S.L., Dietrich, W.E., Donahue, D.J., Jull, A.J.T., and Ribun, M., 1990, Late Quaternary history of
1180 colluvial deposition and erosion in hollows, central California Coast Ranges: *Geological Society*
1181 *of America Bulletin*, v. 102, p. 969-982.

1182 Rhodes, E.J., 2015, Dating sediments using potassium feldspar single-grain IRSL: Initial methodological
1183 considerations: *Quaternary International*, v. 362, p. 14-22.

1184 Rhodes, E.J., 2011, Optically stimulated luminescence dating of sediments over the past 200,000 years:
1185 *Annual Review of Earth and Planetary Sciences*, v. 39, p. 461-488.

1186 Riebe, C.S., Kirchner, J.W., Granger, D.E., and Finkel, R.C., 2001, Minimal climatic control on erosion
1187 rates in the Sierra Nevada, California: *Geology*, v. 29, p. 447-450.

1188 Scherler, D., Munack, H., Mey, J., Eugster, P., Wittmann, H., Codilean, A.T., Kubik, P., Strecker, M.R.,
1189 2014, Ice dams, outburst floods, and glacial incision at the western margin of the Tibetan Plateau:
1190 A >100 k.y. chronology from the Shyok Valley, Karakoram: *Geological Society of America*
1191 *Bulletin*, v. 126(5-6), p. 738-758.

1192 Scherler, D., Bookhagen, B., Wulf, H., Preusser, F., Strecker, M.R., 2015, Increased Late Pleistocene
1193 erosion rates during fluvial aggradation in the Garhwal Himalaya, northern India: *Earth and*
1194 *Planetary Science Letters*, v. 428, p. 255-266, doi: 10.1016/j.epsl.2015.06.034.

1195 Schlunegger, F., Badoux, A., McArdeell, B.W., Gwerder, C., Schnydrig, D., Rieke-Zapp, D., and Molnar,
1196 P., 2009, Limits of sediment transfer in an alpine debris-flow catchment, Illgraben, Switzerland:
1197 *Quaternary Science Reviews*, v. 28, p. 1097-1105.

1198 Schwanghart, W., and Scherler, D., 2014, Short Communication: TopoToolbox 2 – MATLAB-based
1199 software for topographic analysis and modeling in Earth surface sciences: *Earth Surface*
1200 *Dynamics*, v. 2, p. 1–7, doi:10.5194/esurf-2-1-2014.

1201 Sharp, R.P., Allen, C.R., and Meier, M. F., 1959, Pleistocene glaciers on southern California mountains:
1202 *American Journal of Science*, v. 257, p. 81-94,

1203 Shreve, R.L., 1959, Geology and mechanics of the Blackhawk landslide, Lucerne Valley, California [PhD
1204 Thesis]: Pasadena, California Institute of Technology, 79 p.

1205 Spotila, J.A., and Sieh, K., 2000, Architecture of transpressional thrust faulting in the San Bernardino
1206 Mountains, southern California, from deformation of a deeply weathered surface: *Tectonics*, v.
1207 19(4), p. 589–615.

1208 Spotila, J.A., House, M.A., Blythe, A.E., Niemi, N.A., Bank, G.C., 2002, Controls on erosion and
1209 geomorphic evolution of the San Bernadino and San Gabriel Mountains, southern California, in
1210 Barth, A., ed., Contributions to Crustal Evolution of the Southwestern United States: Boulder,
1211 Colorado, Geological Society of America Special Paper 365, p. 205-230.

1212 Stock, J.D., and Dietrich, W.E., 2006, Erosion of steepland valleys by debris flows: Geological Society of
1213 America Bulletin, v. 118(9/10), p. 1125-1148.

1214 Stock, J.D., and Dietrich, W.E., 2003, Valley incision by debris flows: Evidence of a topographic signature:
1215 Water Resources Research, v. 39, p. 1089, doi:10.1029/2001WR001057

1216 Stone, J.O., 2000, Air pressure and cosmogenic isotope production: Journal of Geophysical Research, v.
1217 105, p. 23,753–23,759.

1218 Takahashi, T., 2014, Debris Flow: Mechanics, Prediction and Countermeasures: 2nd edition, CRC Press,
1219 572 p.

1220 Tchakerian, V.P., and Lancaster, N., 2002, Late Quaternary arid/humid cycles in the Mojave Desert and
1221 western Great Basin of North America: Quaternary Science Reviews, v. 21, p. 799-810.

1222 Van der Woerd, J., Klinger, Y., Sieh, K., Tapponnier, P., Ryerson, F.J., and Mériaux, A.-S., 2006, Long-
1223 term slip rate of the southern San Andreas Fault from 10Be-26Al surface exposure dating of an
1224 offset alluvial fan: Journal of Geophysical Research, v. 111, B04407, doi:10.1029/2004JB003559.

1225 Weldon, R.J., II, 1986, The Late Cenozoic geology of Cajon Pass; implications for tectonics and
1226 sedimentation along the San Andreas Fault [PhD Thesis]: Pasadena, California Institute of
1227 Technology, 425 p.

1228 Weldon, R.J., II, and Sieh, K. E., 1985, Holocene rate of slip and tentative recurrence interval for large
1229 earthquakes on the San Andreas fault, Cajon Pass, southern California: Geological Society of
1230 America Bulletin, v. 96, p. 793-812.

1231 Weldon, R., Scharer, K., Fumal, T., Biasi, G., 2004, Wrightwood and the earthquake cycle: What a long
1232 recurrence record tells us about how faults work: GSA Today, v. 14, p. 4-10, doi: 10.1130/1052-
1233 5173(2004)014<4:WATECW>2.0.CO.

1234 Whipple, K.X., and Dunne, T., 1992, The influence of debris-flow rheology on fan morphology, Owens
1235 Valley, California: Geological Society of America Bulletin, v. 104, p. 887-900.

1236 Wobus, C., Whipple, K.X., Kirby, E., Snyder, N., Johnson, J., Spyropolou, K., Crosby, B., and Sheehan,
1237 D., 2006, Tectonics from topography: Procedures, promise, and pitfalls, in Willett, S.D., et al.,
1238 eds., Tectonics, Climate, and Landscape Evolution: Geological Society of America Special Paper
1239 398, Penrose Conference Series, p. 55–74, doi: 10.1130/2006.2398(04).

1240 Zerathe, S., Lebourg, T., Braucher, R., Bourlès, D., 2014, Mid-Holocene cluster of large-scale landslides
1241 revealed in the Southwestern Alps by 36Cl dating. Insight on an Alpine-scale landslide activity:
1242 Quaternary Science Reviews, v. 90, p. 106-127.

1243
1244

1245

1246 **TABLES**1247 **Table 1:** Grain-size counting results

Location	n	Grain size (mm)		
		D ₁₆	D ₅₀	D ₈₄
North Fork San Gabriel Canyon				
Near Crystal Lake (channel)	123	9	35	150
Km 7 (channel)	191	11	215	586
Km 2.3 (flood plain)	100	10	31	128
Km 2.3 (terrace T3)	137	4	20	121
SC* (channel)	97	8	120	406
T1* (terrace)	99	9	23	55
T3* (terrace)	98	8	60	174
T7* (terrace)	100	6	22	73
T8*(terrace)	97	6	38	183
Bear Creek				
Km 3.3 (flood plain)	111	15	34	59
Km 2.9 (flood plain)	117	12	23	52

1248 * Based on grain-size histograms given in Bull (1991).

1249

1250 **Table 2:** Single grain K-feldspar post-IR IRSL age estimates

Sample ID	Lab code	Depth	Elevation	Number of dated grains	Number of dated grains used for age estimate	Dose rate ^a	Equivalent dose ^a	Age ^a
			(m)			(mGy yr ⁻¹)	(Gy)	(ka)
SG13-01	J0525	25	576	36	6	3.67 ± 0.23	27.1 ± 2.4	7.4 ± 0.8
SG13-02	J0526	25	576	46	7	3.68 ± 0.23	27.5 ± 2.1	7.5 ± 0.7
SG13-03	J0527	20	571	116	1	3.94 ± 0.35	22.1 ± 4.7	5.6 ± 1.3
SG13-04	J0528	4	813	109	4	4.39 ± 0.27	35.8 ± 4.0	8.2 ± 1.0
SG13-05	J0529	4	813	25	2	4.27 ± 0.25	29.8 ± 7.2	7.0 ± 1.7

1251 ^a Errors reflect 1-σ uncertainties.

1252

1253 **Table 3:** ¹⁰Be sample details and analytical results

Sample ID	Latitude	Longitude	Elevation above sea level	Boulder dimensions			Mean sample thickness	Topo-graphic shielding	¹⁰ Be concentration ^{ab}	Exposure age ^c
				Height	Width	Length				
	(°N)	(°W)	(m)	(m)	(m)	(m)	(cm)	(atoms/g Qz)	(ka)	
DS103	34.3157	117.8468	1730	1.7	2.5	3	8	1.000	52181 ± 1821	4.0 ± 0.4
DS106	34.3153	117.8445	1702	1.9	2.5	3	5	0.998	49143 ± 1752	3.7 ± 0.3
DS203	34.3055	117.8466	1422	4	4.5	7.5	7.5	0.998	55599 ± 2586	5.0 ± 0.5
DS206	34.3062	117.8528	1603	1.5	2	2	5.5	0.985	449291 ± 8980	32.7 ± 2.9
DS303	34.2815	117.8442	928	1.6	2	2	7	1.000	68496 ± 2225	8.5 ± 0.8
DS304	34.2815	117.8441	930	2	2.8	3	4.5	1.000	64201 ± 6054	7.7 ± 1.0
DS305	34.2814	117.8440	929	1	1.5	3	3.5	1.000	75754 ± 3040	9.1 ± 0.9
DS402	34.2900	117.8355	1074	3	2.5	3	3	0.997	6997 ± 868	0.8 ± 0.1
DS403	34.2910	117.8349	1096	1.5	2	2.5	7	1.000	9066 ± 759	1.0 ± 0.1
DS404	34.3066	117.8426	1426	3.5	2.5	3	3	0.998	46803 ± 2387	4.2 ± 0.4
DS405	34.3065	117.8427	1424	2	2.5	6	7	1.000	43610 ± 1946	4.0 ± 0.4
DS406	34.3123	117.8369	1536	6	5	6	3.5	0.997	49394 ± 1491	4.1 ± 0.4
DS502	34.2881	117.8233	1420	3	4	2.5	10	0.908	7661 ± 3283	0.8 ± 0.3
DS503	34.2894	117.8238	1361	1.6	2	2.5	2	0.952	6720 ± 3031	0.6 ± 0.3

DS504	34.2887	117.8257	1377	1	2.4	2.8	10	0.999	7179 ± 3671	0.7 ± 0.3
-------	---------	----------	------	---	-----	-----	----	-------	-------------	-----------

1254
1255
1256
1257
1258
1259

^a The subtracted laboratory process blank ¹⁰Be/⁹Be ratios are 5.5 × 10⁻¹⁵ (DS103-DS305) and 3.8 × 10⁻¹⁵ (DS402-DS504). ¹⁰Be/⁹Be ratios were normalized to the ¹⁰Be standard 07KNSTD with a nominal ¹⁰Be/⁹Be ratio of 2.85 × 10⁻¹² (Nishiizumi et al., 2007).

^b ¹⁰Be concentration uncertainties reflect total analytical uncertainties at 1-σ level.

^c Exposure ages with external uncertainties based on a time-dependent version (Balco et al., 2008) of the production rate scaling model by Lal (1991) and Stone (2000)

1260 **FIGURE CAPTIONS**

1261

1262 **Fig. 1: Geographical overview of the study area.** (A) Hillshade map of the San Gabriel
1263 Mountains in the western Transverse Ranges. Inset shows State of California with the
1264 trace of the San Andreas Fault (SAF). (B) Hillshade map of the North Fork San Gabriel
1265 and the Bear Creek Canyons. Dotted polygons denote landslide deposits and thin black
1266 lines are faults (Morton and Miller, 2006). (C) Topographic profiles across parts of the
1267 Bear Creek and North Fork San Gabriel Canyons. See (B) for location.

1268

1269 **Fig. 2: River terraces in the North Fork San Gabriel and Bear Creek Canyons.**

1270 Hillshade map color-coded by hillslope angles showing the lower parts of the North Fork
1271 San Gabriel and Bear Creek Canyons.

1272

1273 **Fig. 3: Field photographs of the valley floor and terrace deposits in the North Fork**
1274 **San Gabriel Canyon.** (A) Boulder levee adjacent to the active channel (to the right,

1275 where trees grow). (B) Close-up of debris-flow channel near the debris-flow snout. (C)

1276 Exposure of poorly sorted, matrix supported valley-floor sediments near the active

1277 channel. (D) Close-up of outcrop shown in C. (E) Fill terrace (T7) at Tecolote Flat (see

1278 **Fig. 2** for location), showing poor sorting, but vertical variations in grain size. (F) Close-

1279 up of outcrop shown in E, showing sub-angular clasts in fine-grained matrix, similar to

1280 outcrop in D.

1281

1282 **Fig. 4: Longitudinal profiles of the North Fork San Gabriel and Bear Creek**

1283 **drainage networks.** Inset figures show best fitting χ -transformed drainage networks and

1284 the resulting slope-area scaling. See text for details.

1285

1286 **Fig. 5: Terrace-surface elevations** along the North Fork San Gabriel River (A), the Bear
1287 Creek (B) and the West Fork of the San Gabriel River (C). In each panel, the lower part
1288 shows terrace surfaces that have been projected into a plane following the rivers. The
1289 upper part shows the corresponding interpretation of correlated terrace trends. Inset to
1290 lower right shows smoothed histogram (0.1-m bins) of terrace surface heights above
1291 present-day rivers. Gray rectangles in C denote the expected position of terrace surfaces
1292 joining from the North Fork San Gabriel and Bear Creek Canyons. Estimated bedrock
1293 elevation in A is derived from reconstruction shown in Fig. 7B. See text for details.
1294

1295 **Fig. 6: Comparison of downstream gradients of present-day river and terrace**
1296 **surfaces** (A) in the North Fork San Gabriel Canyon between 0 and 6.7 km upstream
1297 distance from the outlet, and (B) in the Bear Creek Canyon between 0 and 10 km
1298 upstream distance from the outlet. Size and color coding of the marker symbols is the
1299 same in both panels. Downstream elongation is defined as the ratio of the downstream
1300 and the across-stream extent.
1301

1302 **Fig. 7: Estimated valley-fill thickness in the North Fork San Gabriel Canyon.** (A)
1303 The eroded valley-fill thickness corresponds to the elevation difference between the
1304 reconstructed T7 terrace level and the present-day topography. (B) The total valley-fill
1305 thickness is the elevation difference between the reconstructed T7 terrace level and the
1306 reconstructed bedrock at the base of the valley fill. Black lines delineate T7 terrace
1307 surfaces.
1308

1309 **Fig. 8: River terraces in the North Fork San Gabriel Canyon.** (A) View upstream
1310 from road near Tecolote Flat. T4, T7, and T8 denote terrace levels originally defined by
1311 Bull (1991). The river is concealed by bare-branched trees. (B) Fill terrace outcrop at
1312 Tecolote Flat. Dashed white line marks boundary that was proposed by Bull (1991),
1313 between a stratigraphically older (T3) and younger valley fill (T7). See the
1314 supplementary material for a color version of the photograph in **Fig. 8B**.
1315

1316 **Fig. 9:** Grain size distributions for modern river and terrace sediments. Question marks
1317 behind ‘T3’ indicate uncertainty whether this deposit is truly different from T7. See text
1318 for details.

1319

1320 **Fig. 10: Apparent age and probability density functions of single grain IRSL**
1321 **determinations** (all results in grey; grains selected for age estimation in black). The text
1322 inside the axes provides the sample ID and the number of grains that produced a finite
1323 age estimate (top row), the depositional age with 1- σ uncertainties obtained from selected
1324 grains highlighted in black (middle row), and the number of grains contributing to the age
1325 (bottom row). The samples are dominated by a broad distribution of many unbleached or
1326 poorly bleached grains, and a young age peak. See text for details.

1327

1328 **Fig. 11: Map of landslide deposits in the headwaters of the North Fork San Gabriel**
1329 **Canyon.** Upper right inset shows tentative chronology of landslide events, constrained by
1330 ^{10}Be -surface exposure ages. Topographic profile a-a’ shown in **Fig. 16**.

1331

1332 **Fig. 12: Morphology of the Alpine Creek landslide.** (A) Hillshade map showing
1333 landslide deposits (dotted), topographic ridges (dashed black lines), and trace of
1334 topographic profiles (solid black lines). Triangles indicate dated boulders. Contour
1335 interval is 50 m. (B) Longitudinal profile along channel, marked x-x’ in A. Gray areas
1336 denote incision of channel into bedrock and landslide deposits, as obtained from white
1337 profile next to the channel in A. Position of transverse profiles shown in C are marked by
1338 lower case letters (a-f). (C) Topographic profiles transverse to the downvalley direction.
1339 Thick gray lines mark distribution of landslide deposits.

1340

1341 **Fig. 13: Landslide boulders.** (A) Typical granitic-gneissic boulder that was sampled for
1342 surface exposure dating (DS403). Boulder height is ~1.5 m. (B) Boulder field atop
1343 topographic ridge associated to the Alpine Canyon landslide, near sample DS503. View
1344 is to the southwest. Field of view in the center of the photograph is ~150 m.

1345

1346 **Fig. 14: Field photograph of the Alpine Canyon landslide and Clouburst Canyon.**
1347 The landslide surface has been dissected by ~35 m. Star indicates sampled boulders with
1348 an exposure age of $\sim 0.9 \pm 0.1$ ka.

1349

1350 **Fig. 15: Sample ages and combined probability density function for landslide**
1351 **boulders (solid) and terrace sediments (hollow) in the North Fork San Gabriel**
1352 **Canyon.** Post-IR IRSL (squares) and ^{10}Be ages (circles) from this study, ^{14}C ages
1353 (triangles) from Bull (1991). Error bars reflect $1-\sigma$ (IRSL, ^{14}C) and external uncertainties
1354 (^{10}Be ; c.f., Balco et al., 2008).

1355

1356 **Fig. 16: Topographic profile across the Crystal Lake landslide.** Solid black line gives
1357 elevation along profile a-a' shown in **Fig. 11**. Bold gray line indicates landslide deposits,
1358 broken where inferred. Thalweg and ridgeline elevations are projected into the profile.

1359

1360 **Fig. 17:** Sketch of fill-terrace formation by debris flows due to sediment supply from a
1361 large landslide.

1362

1363 **Fig. 18: Map of the San Gabriel Mountains** showing 2-km radius local relief (grayscale
1364 colors), catchment boundaries (thick white lines), selected mountain peaks (triangles), the
1365 landslide deposits in the North Fork San Gabriel Canyon (thin white lines), potentially
1366 seismogenic faults (black lines), and locations of debris flow catchments shown in Fig.
1367 19.

1368

1369 **Fig. 19: Oblique aerial views of active (A, B) and inactive (C, D) debris flow**
1370 **catchments in the San Gabriel Mountains.** Vertical arrows indicate sediment source
1371 areas, horizontal arrows indicate debris flow deposits. Distance from source area to toe of
1372 debris flow deposits is approximately 9 km (A), 4 km (B), 2 km (C), and 4 km (D). All
1373 images from Google Earth.

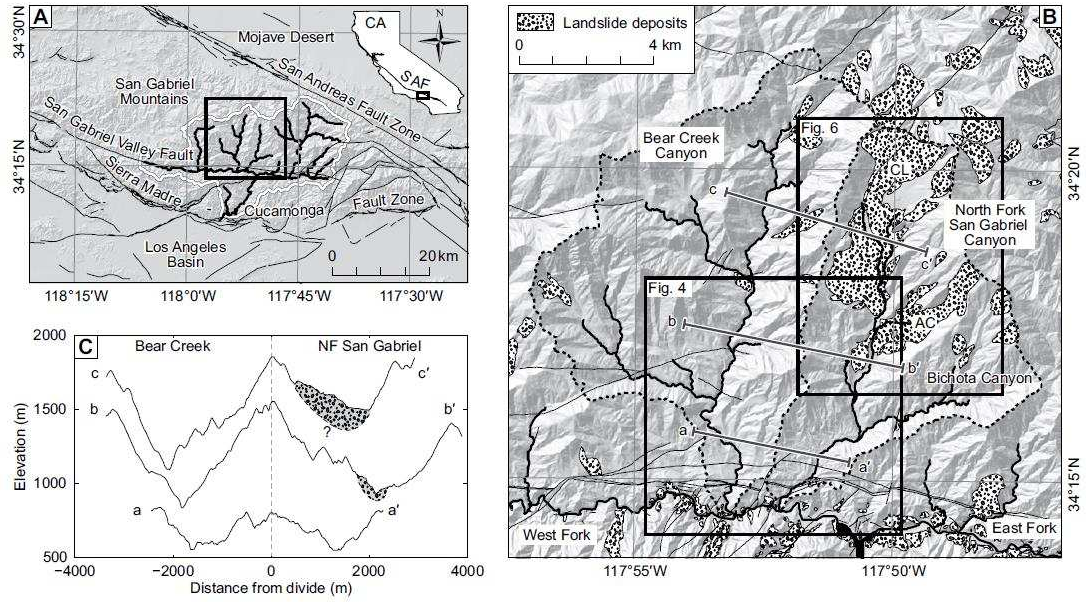
1374

1375

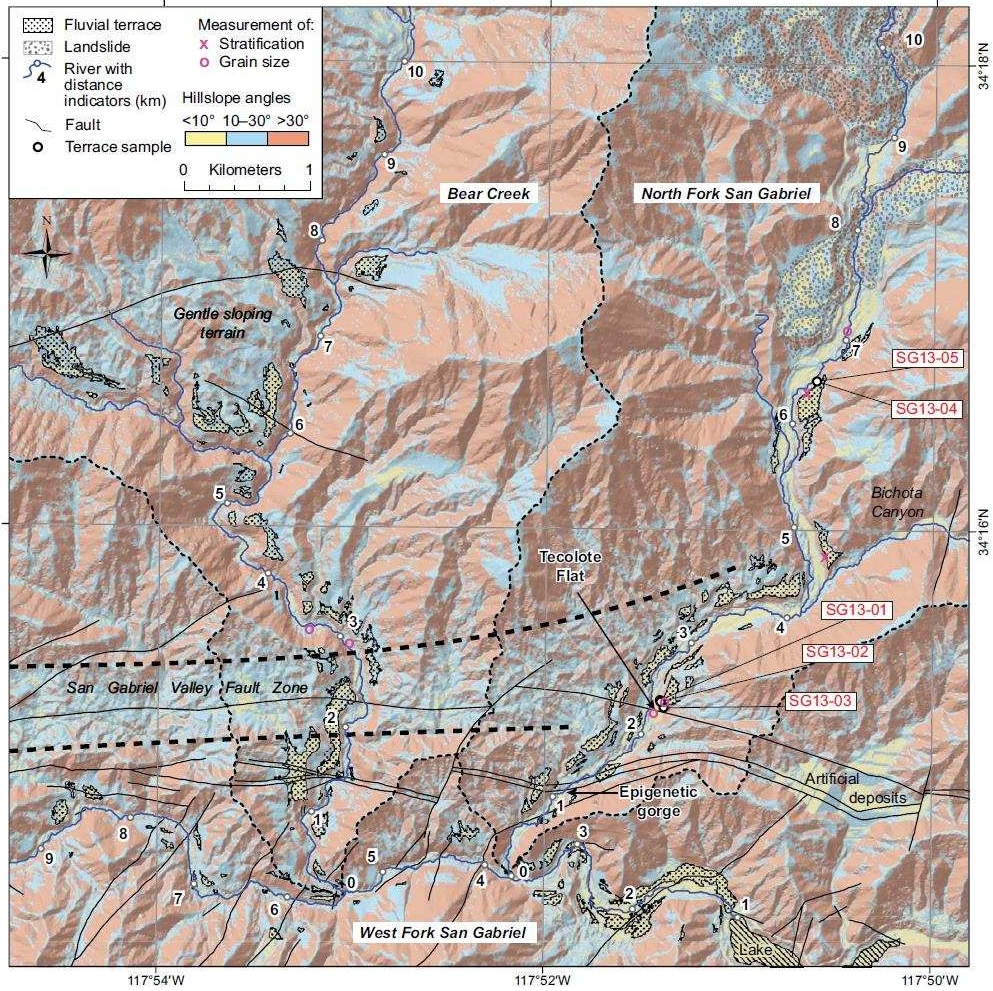
1376

1377
1378
1379

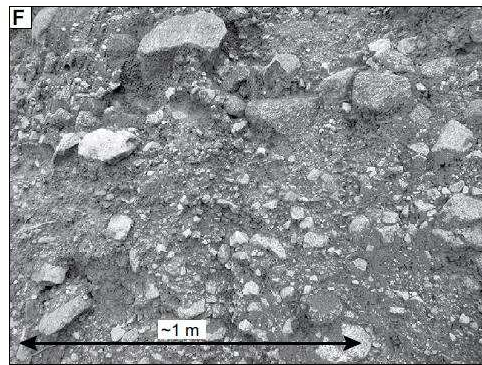
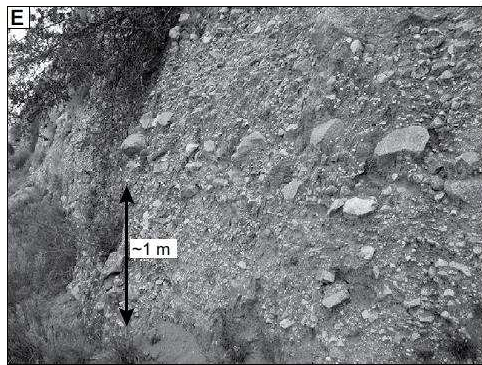
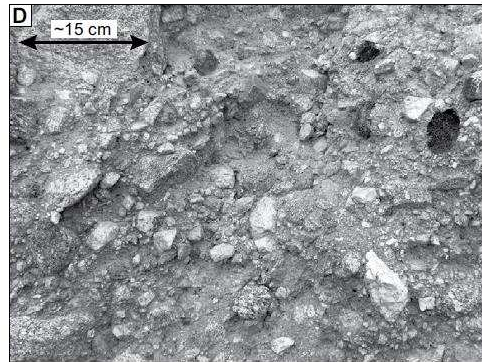
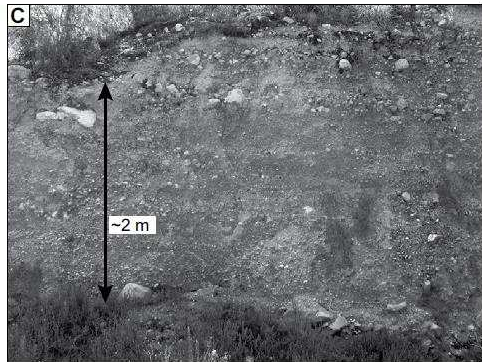
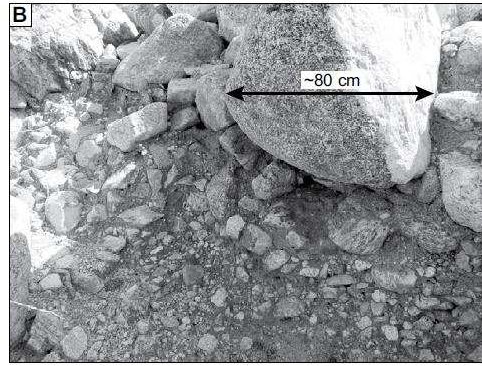
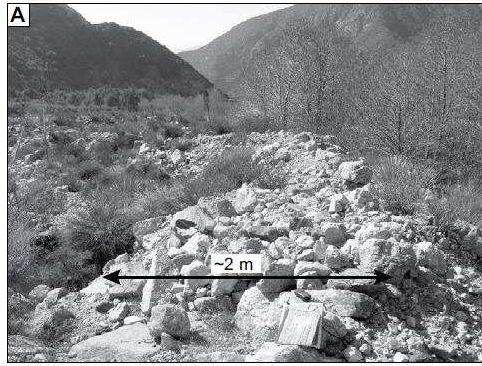
Figs. 1 to 19 below in order



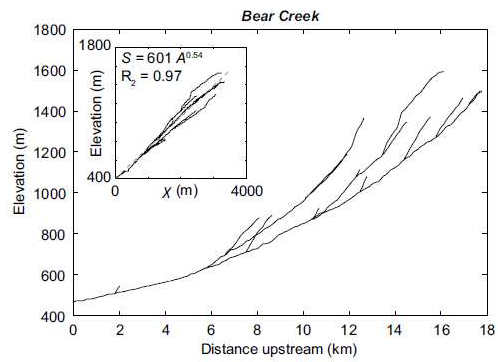
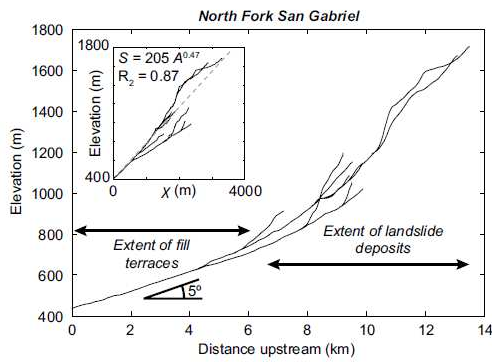
1380
1381



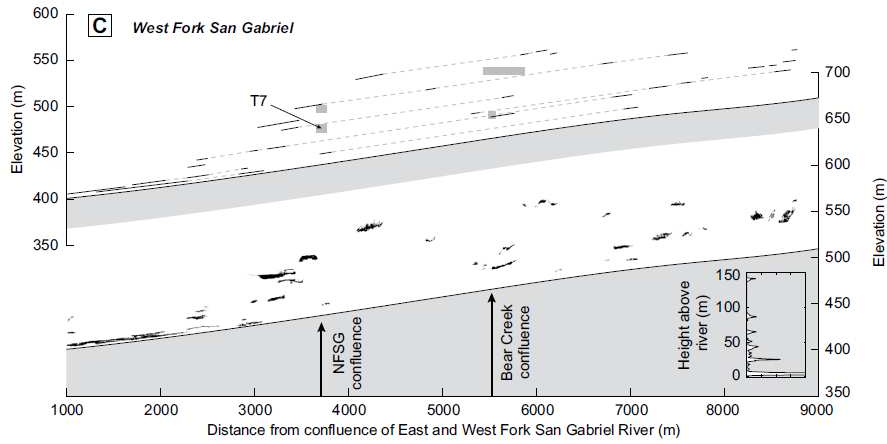
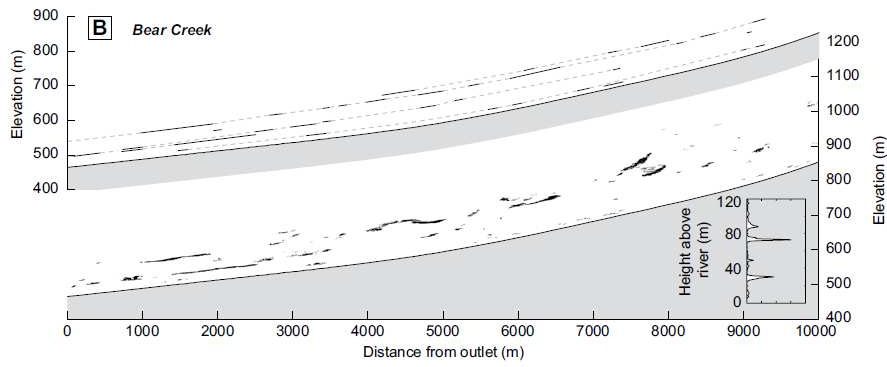
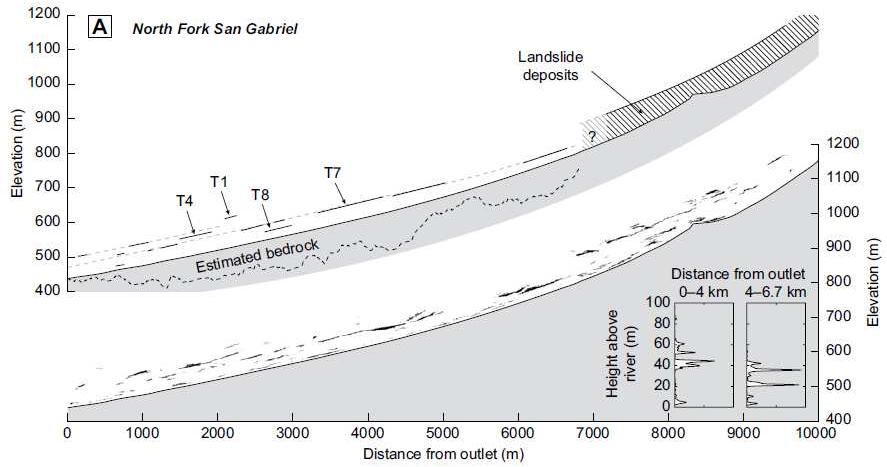
1382



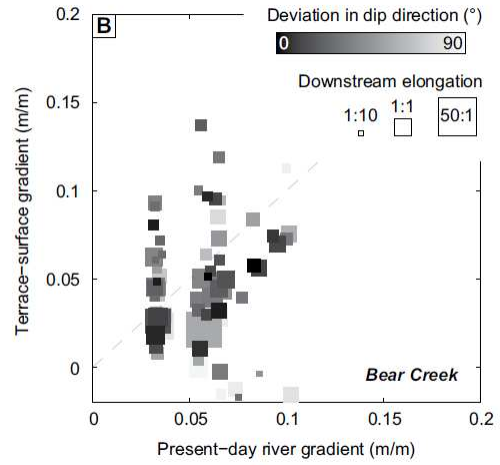
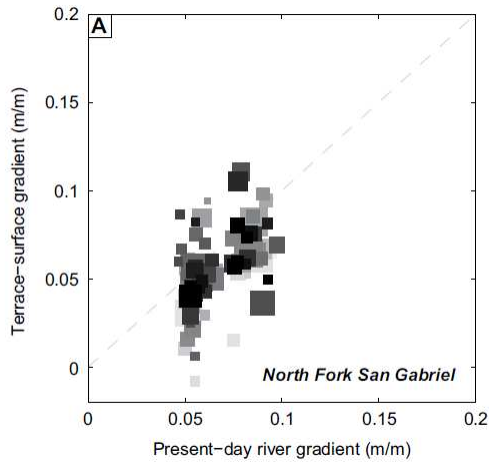
1383



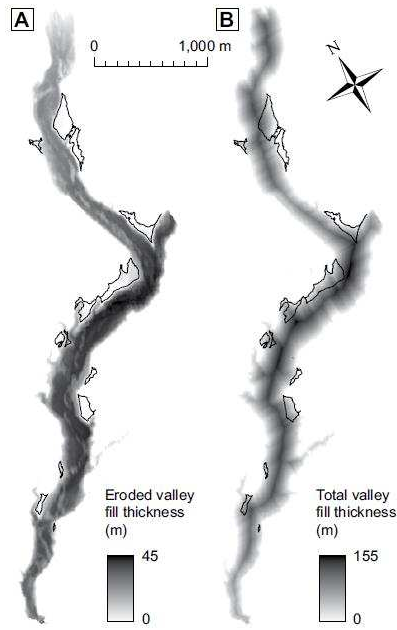
1384



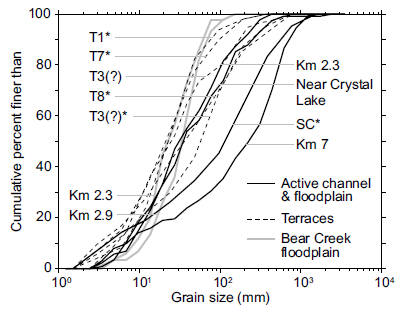
1385



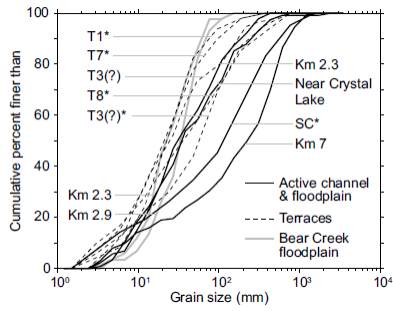
1386



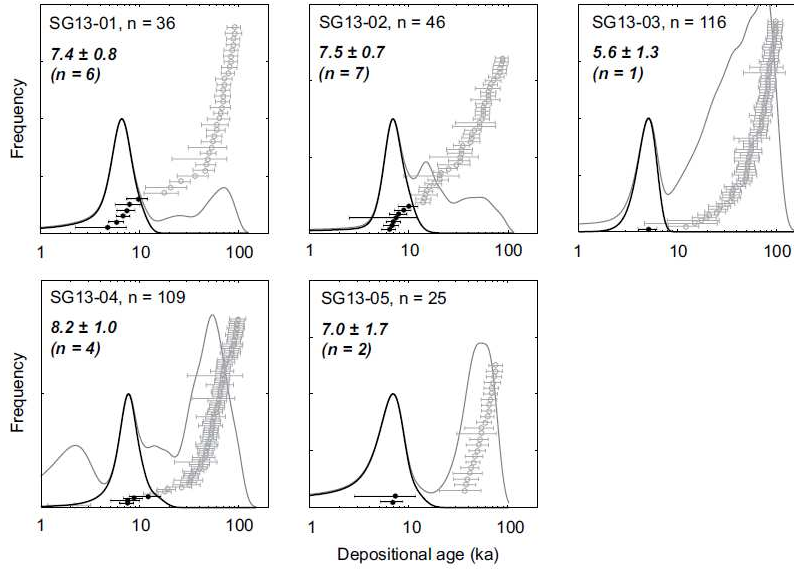
1387



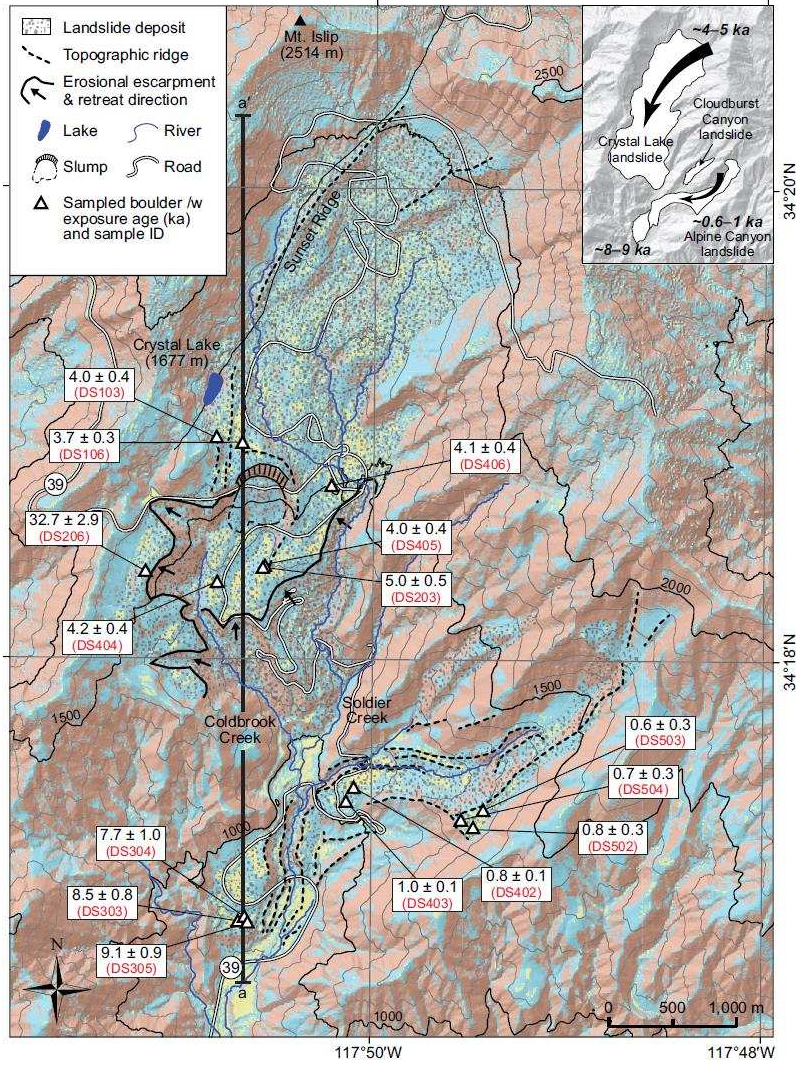
1388



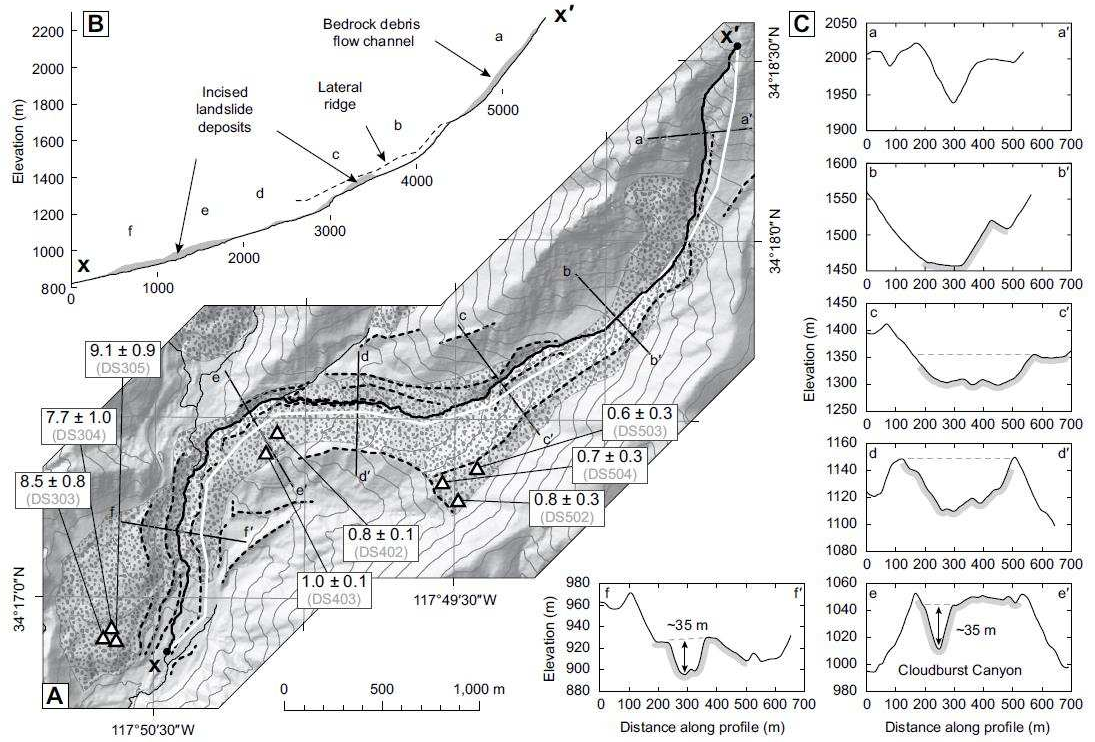
1389



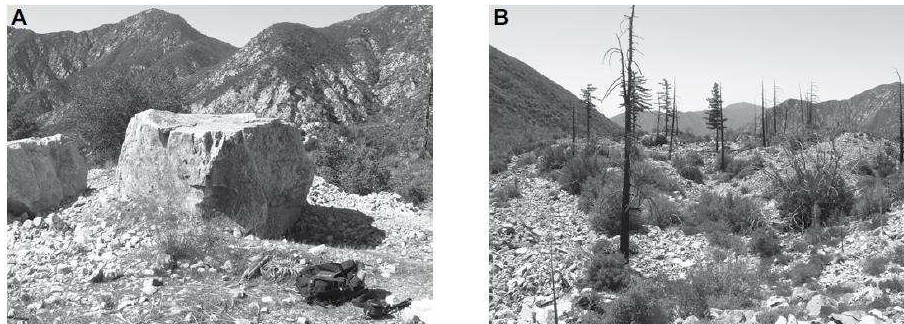
1390



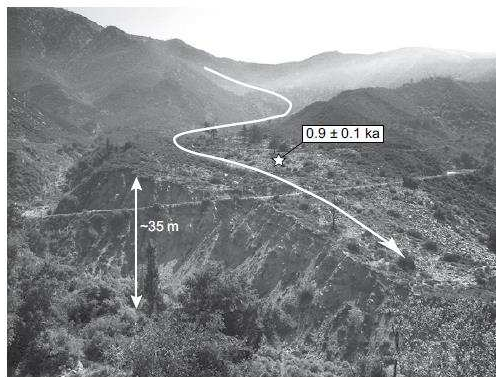
1391



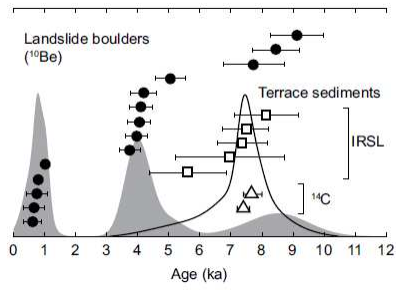
1392



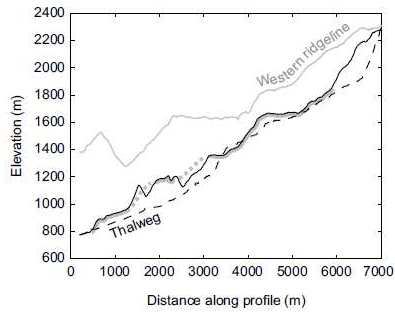
1393



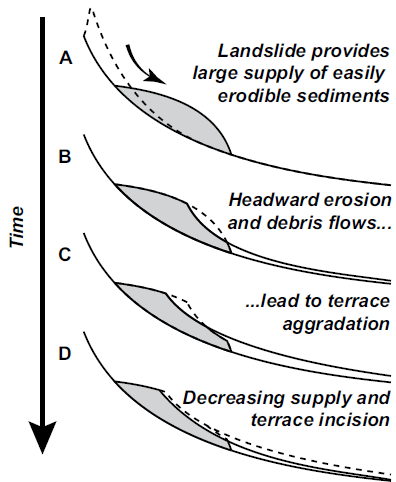
1394



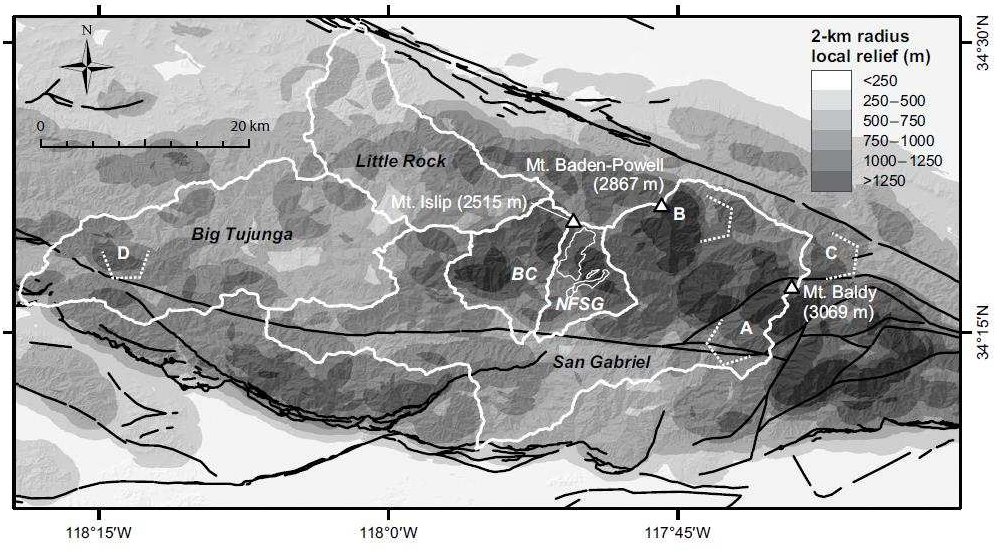
1395



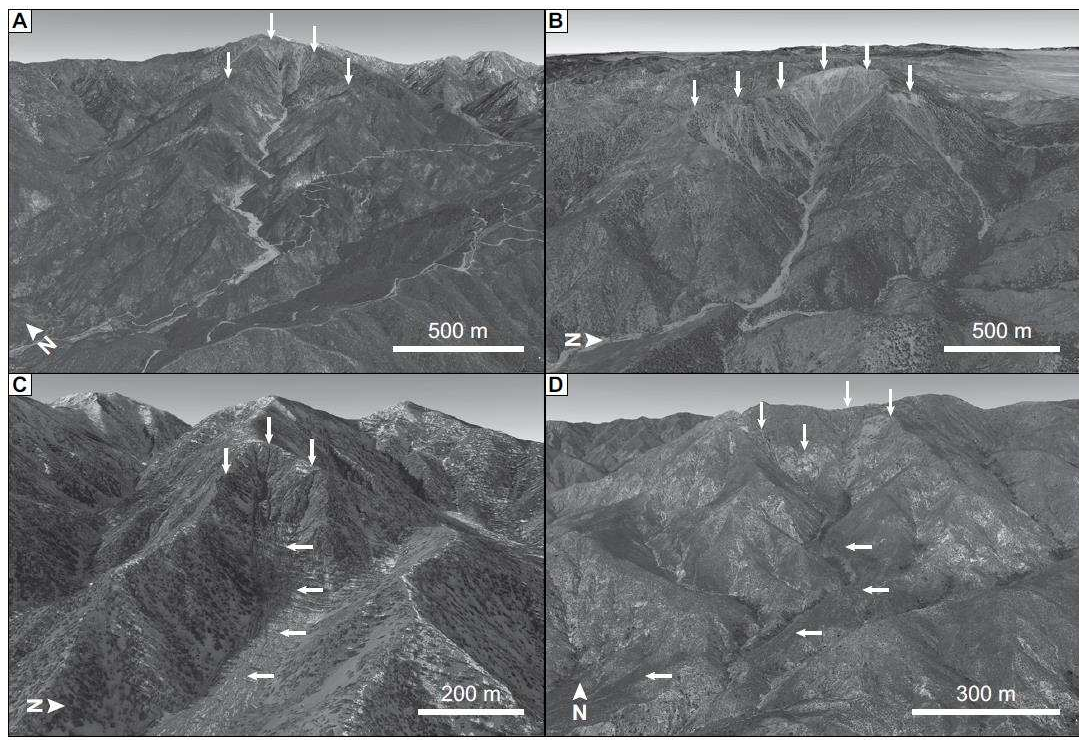
1396



1397



1398



1399